haematologica
Journal of the Ferrata Storti Foundation

Splenic erythrophagocytosis is regulated by ALX/FPR2 signaling

by Haley Asplund, Hector H. Dreyer, Jing-Juan Zheng, Richa Singhal, Jason L. Hellmann and Brian E. Sansbury

Received: April 11, 2025.
Accepted: August 29, 2025.

Citation: Haley Asplund, Hector H. Dreyer, Jing-Juan Zheng, Richa Singhal, Jason L. Hellmann and Brian E. Sansbury. Splenic erythrophagocytosis is regulated by ALX/FPR2 signaling. Haematologica. 2025 Sept 11. doi: 10.3324/haematol.2025.288007 [Epub ahead of print]

Splenic erythrophagocytosis is regulated by ALX/FPR2 signaling

Haley Asplund[1], Hector H. Dreyer[1], Jing-Juan Zheng[1], Richa Singhal[1], Jason L. Hellmann[1], and Brian E. Sansbury[1]

1. Center for Cardiometabolic Science, Christina Lee Brown Envirome Institute, Division of Environmental Medicine, Department of Medicine, University of Louisville, Louisville, Kentucky, USA.

Disclosures: Support for this work was provided by the NIH (R01ES034389; R01GM127495; P30GM127607). Computational resources and bioinformatics pipelines were provided by the KY INBRE Bioinformatics Core with funding from the National Institute of General Medical Sciences, NIH (P20GM103436). Its contents are solely the responsibility of the authors and do not necessarily represent the official views of the NIH.

Contributions: H.A., H.H.D., J.J.Z., R.S. performed experiments, analyzed data, and wrote the manuscript. J.L.H. designed experiments, supervised research, and wrote the manuscript. B.E.S. conceived and planned the project, supervised research, analyzed data, and wrote the manuscript. B.E.S. is the guarantor of this work and, as such, had full access to the data and takes responsibility for the integrity of the data and the accuracy of the data analysis.

Data-sharing statement: RNA-seq data have been deposited in the NCBI GEO database with the accession numbers GSE292685 and GSE292686.

Short Title: ALX/FPR2 regulates erythrophagocytosis

Keywords: proresolving lipid mediators, red pulp macrophages, red blood cell turnover

Correspondence to:

Brian E. Sansbury
Brian.Sansbury@Louisville.edu
580 S. Preston St., Room 304D
Louisville, KY 40202

Abstract:

Maintaining a healthy pool of circulating red blood cells (RBCs) is essential for adequate perfusion, as even minor changes in the population can impair oxygen delivery, resulting in serious health complications including tissue ischemia and organ dysfunction. This responsibility largely falls to specialized macrophages in the spleen, known as red pulp macrophages, which efficiently take up and recycle damaged RBCs. However, questions remain regarding how these macrophages are acutely activated to accommodate increased demand. Proresolving lipid mediators stimulate macrophage phagocytosis and efferocytosis but their role in erythrophagocytosis has only recently been described. To investigate the role of lipid mediators on red pulp macrophage function, we targeted the ALX/FPR2 signaling pathway, as this receptor binds multiple lipid mediator ligands eliciting potent macrophage responses. We found that mice with *Fpr2* deletion exhibited disrupted erythrocyte homeostasis resulting in an aged RBC pool, decreased markers of splenic RBC turnover, and altered splenic macrophage phenotype characterized by changes in heme metabolism. Upon activation of on-demand erythrophagocytosis, production of the ALX/FPR2 ligand, lipoxin A_4 (LXA_4), was induced in the spleen while receptor-deficient animals were unable to efficiently clear damaged RBCs, a defect that was conserved in mice with myeloid-specific *FPR2* deletion. Similarly, mice lacking the LXA_4 biosynthetic enzyme displayed defective erythrophagocytosis that was rescued with LXA_4 administration. These results indicate that the ALX/FPR2 signaling axis is necessary for maintenance of RBC homeostasis and LXA_4 activation is a critical aspect of the red pulp macrophage response to acute erythroid stress.

1. Introduction

Red blood cells (RBCs) are the most abundant cell type in the body and are traditionally appreciated for their role in respiration and gas exchange. Recently, RBCs have garnered new attention for their immunomodulatory effects which are primarily achieved via their interaction with resident macrophages in the spleen—known as red pulp macrophages (RPM).[1,2] As erythrocytes enter the spleen, RPM probe the cells for signs of mechanical and oxidative damage, as well as inflammatory stimuli bound to cell surface receptors (e.g., foreign pathogens, endogenous chemokines).[1] Once recognized, RPM prune damaged portions of erythrocyte membranes or phagocytose the cell entirely, efficiently processing and recycling the cellular cargo.[3] In a healthy human this process—termed erythrophagocytosis—accounts for the daily turnover of roughly 150-200 billion RBCs.[3,4] Consequently, defects in the system can impact physiological iron recycling and induce wide-ranging health effects including anemia, impaired host defense, and even sepsis.[2]

While much is known about the process of erythrophagocytosis, critical questions remain regarding the fundamental regulatory mechanisms that govern its activation and function. Of particular interest is the RPM response to increased erythrophagocytic demand as may be encountered during acute hemolytic reactions induced by transfusions,[5,6] infection,[7] autoimmunity,[8] or genetic disorders.[9] Addressing these gaps in knowledge presents a significant opportunity for developing therapeutics for conditions like transfusion-related immunomodulation and sickle cell disease.

Lipid mediators derived from the enzymatic conversion of polyunsaturated fatty acids (PUFA) are a newly appreciated class of autacoid signaling molecules that have

dramatic impacts on immune cells, including macrophages.[10,11] In particular, specialized proresolving lipid mediators (SPM) bind G protein-coupled receptors—like ALX/FPR2—on macrophages enhancing migration, phagocytosis, and efferocytosis while limiting proinflammatory cytokine production, thereby promoting the active resolution of inflammation.[12-16] SPM activation of ALX/FPR2 is linked to improvements in numerous inflammatory conditions (i.e., atherosclerosis, heart failure, diabetes[17,18]) and, as we have demonstrated, plays a vital role in hastening tissue repair processes after injury.[19-21]

While the role of the SPM-ALX/FPR2 signaling axis in promoting macrophage clearance of pathogens, debris, apoptotic cells is well documented, its impact on RBC disposal has only recently been demonstrated.[22,23] These studies establish the foundation that SPM, including ligands of ALX/FPR2, are involved in macrophage-mediated RBC clearance, however, it remains incompletely understood whether ALX/FPR2 signaling contributes to basal erythroid homeostasis and what role its activation plays during cases of acutely increased erythrophagocytosis.

Here, we present evidence that the ALX/FPR2 receptor is required for optimal homeostatic RBC turnover and is critical in facilitating splenic macrophage-mediated erythrophagocytosis. These results demonstrate the importance of the ALX/FPR2 signaling axis in coordinating red pulp macrophage function and further illustrate the potent immunomodulatory ability of SPM to govern fundamental physiological processes.

2. Methods

Detailed methods are available in the accompanying Supplementary Materials.

2.1 Animals and Reagents

Male C57BL/6J (#00664), *Spic*-EGFP (#025673), and *Alox15*$^{-/-}$ (#002778) mice were from Jackson Laboratories (Bar Harbor, ME). *Fpr2*$^{-/-}$ and wild type (C57BL/6Ntac) mice were provided by Idorsia Pharmaceuticals and bred on-site. Mice with myeloid-specific deletion of h*FPR2* were generated as previously described[21] by crossing humanized *ALX/FPR2-GFP* floxed mice (provided by Idorsia) with commercially available LysM-Cre mice (Jackson; #004781). All procedures were performed in accordance with ethical regulations and pre-approved by the University of Louisville Institutional Animal Care and Use Committee. LXA_4 was purchased from Cayman Chemical (Ann Arbor, MI). Antibodies used for flow cytometry were purchased from BioLegend (San Diego, CA).

2.2 *In vivo* RBC turnover

Biotin was administered i.v. and tail blood sampled serially. RBC biotin expression was determined by flow cytometry.

2.3 RNA-Sequencing

RNA was isolated from mouse spleen and F4/80^{+} splenocytes and subjected to poly-A RNA sequencing. Abclonal second strand synthesis module kit was utilized for library construction. Paired-end sequencing was performed on an Illumina NovaSeq X Plus using the 25B Flow Cell. RNA-seq data have been deposited in the NCBI GEO database with the accession numbers GSE292685 and GSE292686.

2.4 *In vivo* splenic RBC uptake

RBCs from donor mice were oxidized with 0.2 mM copper(ii) sulfate ($CuSO_4$) and 5 mM L-ascorbic acid or incubated with 10 µg/mL CD47 antibody (Bio X Cell) or 10 µg/mL mouse IgG isotype control (Bio X Cell, BE0083). RBC ($2x10^8$ cells) were labeled with carboxyfluorescein succinimidyl ester (CFSE) and administered to mice (i.v.). After 1 hour, spleens were collected.

2.5 *Ex vivo* splenocyte RBC uptake

A single cell suspension was generated from spleens using 70 µM cell strainer with RPMI 1640 supplemented with 10% FBS using the plunger from a 5 mL syringe. The suspension was centrifuged and RBC lysis was performed. The suspension was centrifuged and resuspended in RPMI 1640 with 10% FBS and 2 mM EDTA. Oxidized, CFSE-labeled RBC were added (1:10; splenocyte:RBC ratio) and incubated for 1 hour at 37°C, with gentle agitation every 15 minutes. Tubes were placed on ice to stop phagocytosis, centrifuged, and RBC lysis performed. Samples were centrifuged and resuspended in cell staining buffer prior to antibody staining for flow cytometry analysis.

2.6 Targeted lipidomics

Spleens were placed in methanol containing commercially available deuterium-labeled synthetic standards (PGE_2-d4, 15d-PGJ_2-d4, LTB_4-d4, LXA_4-d5, 11,12-EET-d11, 15-HETE-d8, 5-HETE-d8, RvE1-d4, RvD2-d5, RvD3-d5, MaR1-d5, and MaR2-d5) then stored at -80°C prior to being minced. Samples were acidified and added to C18 SPE columns. Neutral lipids were removed from the column using *n*-hexanes while lipid mediators were eluted with methyl formate. Using N_2 gas, solvent was evaporated and samples resuspended in methanol:water (50:50, v/v). Samples were analyzed using a Shimadzu liquid chromatography system (LC 20-AD with an SIL-20AC autoinjector)

coupled to a QTrap5500 mass spectrometer operated in negative polarity mode. Lipid mediator identification was based on the following criteria: chromatographic peak retention time matching that of synthetic standards run in parallel (+/- 0.1 min); signal:noise ratio >5; and an on-column calculated concentration above the lower limit of quantification for each mediator. Absolute quantification was achieved by comparing samples to a 12-point standard curve of synthetic standards run in parallel. SCIEX OS (v.2.0.1) software was used for peak identification and quantification.

2.7 Statistical Analysis

Data presented as mean ± standard error of the mean. Statistical differences between groups were determined by performing two-tailed unpaired Student's t-test or two-way analysis of variance (ANOVA) using GraphPad Prism version 10. Statistical significance is denoted as: *$p<0.05$, **$p<0.01$, ***$p<0.001$, ****$p<0.0001$, or ns – $p>0.05$. Schematics used in figures were created using BioRender.

3. Results

3.1 Erythroid homeostasis is perturbed in mice lacking the ALX/FPR2 receptor

Previous studies have suggested a link between proresolving lipid mediator ligands of ALX/FPR2 and senescent RBC uptake and disposal.[22,23] To better understand the role of signaling via ALX/FPR2 in basal RBC homeostasis, we questioned whether deletion of the receptor would impact erythrocyte turnover. Using an *in vivo* two-step labeling approach[24] wild type (WT) mice and mice lacking the ALX/FPR2 receptor (*Fpr2*$^{-/-}$) first received a high dose of biotin followed five days later by a second lower dose. This method allows for the relative age of circulating RBCs to be distinguished based on biotin signaling intensity. Over the course of one week following the second biotin administration, we found that the abundance of Biotin^{Hi} cells remained elevated while there was a reduced appearance of Biotin^{Neg} cells in *Fpr2*$^{-/-}$ mice compared with WT (**Fig. 1A,B**), indicating that the rate of RBC turnover was significantly decreased in *Fpr2*$^{-/-}$ mice. To further characterize the state of the circulating erythroid pool in *Fpr2*$^{-/-}$ mice, we investigated the expression of CD47, an important marker of 'self' which is expressed highly on erythroblasts—preventing their premature uptake and clearance—and progressively decreases with age and stress on circulating RBCs.[25] We found lower levels of CD47 in *Fpr2*$^{-/-}$ mice (**Fig. 1C**), indicating an aged RBC population. Additionally, we examined the abundance of circulating reticulocytes as a measure of newly released erythroid cells into circulation and found that these too were decreased in *Fpr2*$^{-/-}$ mice (**Fig. 1D**). To determine whether decreased circulating reticulocytes were a result of changes in erythropoiesis, we analyzed erythroid precursor populations in the bone marrow of WT and *Fpr2*$^{-/-}$ mice. Interestingly, we found that the number of total erythroblasts and reticulocytes was not different between strains but the distribution of

subpopulations was altered suggesting potential dysregulation in the erythroblast maturation process and release of reticulocytes into circulation (**Supplementary Fig. 1**). Importantly, we did not detect clear clinical indications of overt anemia in *Fpr2*$^{-/-}$ mice as determined by complete blood count analysis (**Supplementary Fig. 2**), though red cell distribution width (RDW) was trending lower. These findings indicate that deletion of ALX/FPR2 slows the basal rate of erythrocyte turnover, resulting in an aged pool of circulating RBCs.

3.2 *Fpr2*$^{-/-}$ mice have decreased splenic markers of RBC turnover

Given the observed changes in erythroid turnover in mice lacking ALX/FPR2, we asked whether *Fpr2* deletion had specific impacts on the spleen as it is the primary site of RBC disposal and a critical regulator of erythroid homeostasis. Gross examination and gravimetric analysis (spleen/body weight ratio; data not shown) of spleens suggested no differences between WT and *Fpr2*$^{-/-}$ mice. We then performed histological analyses using hematoxylin and eosin-stained tissue sections (**Fig. 2A**) and similarly found that tissue structure was unaltered as quantified by red pulp to white pulp ratio (**Fig. 2B**). Upon closer examination of the tissue, however, we noted an apparent decrease in prevalence of deposits of rich brown staining in the red pulp of *Fpr2*$^{-/-}$ spleens (denoted by arrows in higher magnification images of **Fig. 2A**), which may be indicative of heme or iron deposits. We quantified the abundance of these deposits and found that there were significantly fewer in *Fpr2*$^{-/-}$ spleens (**Fig. 2C**). To further explore whether these deposits reflected areas of red blood cell turnover, we stained the sections with Prussian blue and found these same regions also had increased amounts of iron (**Fig.**

2D). Moreover, when we quantified the total amount of iron positive areas in the sections, we determined that the spleens of *Fpr2*$^{-/-}$ mice had significantly less (**Fig. 2E**). As resident macrophages in the red pulp are the cells chiefly responsible for erythrophagocytosis, we performed F4/80 immunostaining of the tissue and found that, as expected, these areas of heme and iron deposits were also highly enriched in macrophages (**Fig. 2F**). To confirm these histological analyses, we performed a colorimetric biochemical assay and found that the total amount of heme in *Fpr2*$^{-/-}$ spleens was decreased (**Fig. 2G**). These data indicate that there is decreased abundance of the prominent intracellular components of RBCs in the red pulp of spleens of *Fpr2*$^{-/-}$ mice suggesting that macrophage-mediated uptake and breakdown of the cells is reduced.

3.3 Deletion of *Fpr2* alters the transcriptomes of spleen and splenic macrophages

We next sought to define global alterations in the spleen driven by ALX/FPR2 deletion. To address this, we performed RNA-sequencing (RNA-seq) analysis of spleens from WT and *Fpr2*$^{-/-}$ mice (**Fig. 3A**). This analysis revealed 61 differentially expressed genes (DEG; 53 downregulated, 8 upregulated) with *Fpr2*, unsurprisingly being the most significantly affected gene (**Fig. 3B**). Interestingly, *Alox5* and *Alox15* which encode 5-lipoxygenase and 12/15-lipoxygenase, respectively, were also significantly downregulated (**Fig. 3B**). These enzymes are required for the conversion of polyunsaturated fatty acid (PUFA) substrates into proresolving lipid mediators—including LXA_4, a ligand of ALX/FPR2. To better understand the global changes associated with the identified DEG, we performed gene ontology biological processes

(GO:BP) enrichment analysis. Driven largely by *Alox5* and *Alox15*, we found that the Lipoxin Biosynthesis pathway was significantly enriched (**Fig. 3C**). Additional significantly enriched pathways were then clustered based on their biological similarities. Each of these clusters were directly related to innate immune activation and suggested that changes in the myeloid/leukocyte compartment of the tissue were driving the global transcriptomic signature. Macrophages are known sources and targets of SPM, including lipoxins, and are the principal splenic cell type responsible for erythrocyte disposal. Thus, we hypothesized that *Fpr2*$^{-/-}$ deletion acutely targets splenic macrophages.

We isolated F4/80^{+} splenocytes from WT and *Fpr2*$^{-/-}$ mice and performed additional RNA-seq analysis (**Fig. 3D**). Here, we found more sweeping changes than that of the whole spleens with 179 total DEG (94 downregulated, 85 upregulated). However, similar to the spleen analysis, we observed that *Fpr2* was the most significantly changed gene and *Alox5* was also downregulated (*Alox15* expression was decreased, yet not significantly) (**Fig. 3E**). Also similar to the analysis of whole spleen, GO:BP enrichment analysis identified that pathways related to Immune/Inflammatory Response, Defense Response/Response to External Stimuli, and Leukocyte Migration/Chemotaxis were significantly enriched (**Fig. 3F**). Interestingly, however, pathways related to Heme Biosynthesis and Hematopoiesis were also impacted. To understand which significantly changed genes were driving the observed pathway enrichment, we compiled the DEG of each significantly enriched GO pathway and displayed them according to their expression change (**Fig. 3G**). This revealed that the majority of DEG that were related to the Immune/Inflammatory Response, Leukocyte

Migration/Chemotaxis, and Hemopoiesis/Cell Development pathways were downregulated in *Fpr2*$^{-/-}$ mice, while the Defense Response/Response to External Stimuli pathways were represented by DEG that were both upregulated and downregulated. Interestingly, all DEG related to Heme Biosynthesis/Metabolism were upregulated. Considering these data with the histological examination, this may reflect a compensatory induction of genes related to heme balance in *Fpr2*$^{-/-}$ mice. Taken together, these results indicate that deletion of *Fpr2* induces an altered transcriptomic phenotype in splenic macrophages which may impact their ability to effectively respond to inflammatory stimuli or efficiently perform RBC turnover.

3.4 Red pulp macrophages express *Fpr2* and in its absence splenic uptake of stressed RBCs is impaired

Next, we questioned whether the altered transcriptomes observed in spleens and splenic macrophages of *Fpr2*$^{-/-}$ mice lead to functional impairments that may contribute to altered erythrocyte turnover. Recognition and disposal of damaged RBCs is a task primarily performed by red pulp macrophages (RPM), a distinct population of splenic resident macrophages. First, we sought to determine whether RPM express *Fpr2*. To definitively identify the RPM population, we used *Spic*-EGFP reporter mice, as *Spic* is the key transcription factor that controls RPM development[26] (**Fig. 4A**). In spleens of these mice, we found that the GFP^{+} cells were clustered into a distinct population based on expression of CD11b and F4/80 (CD11b^{dim},F4/80^{hi}) while the GFP^{-} cells did not contain this population (**Supplementary Fig. 3**). To further validate that this population was RPM, we performed flow cytometry-based cell sorting of GFP^{+} and GFP^{-}

splenocytes and investigated expression of hallmark RPM genes. As expected, we found that GFP^+ cells expressed significantly higher levels of *Spic*, *Hmox1* (heme oxygenase 1), *Slc40a1* (ferroportin), and *Slc48a1* (heme-responsive gene 1) than GFP^- cells, confirming their identity as RPM (**Fig. 4B**). We then measured expression of *Fpr2* and found that the receptor was also significantly enriched in RPM compared to non-RPM splenocytes (**Fig. 4C**). Interestingly, we also found that expression of *Alox15* was decreased in RPM which may suggest that non-RPM cells are more responsible for SPM production while RPM are targets of SPM actions.

After validating the identification of RPM by flow cytometry and establishing that RPM express *Fpr2*, we next questioned whether the ability to clear RBCs efficiently would be impacted in mice lacking ALX/FPR2. To test this, we performed an *in vivo* splenic RBC disposal assay in WT and $Fpr2^{-/-}$ mice. RBCs from WT donor mice were exposed to an *ex vivo* oxidative insult ($CuSO_4$) prior to labelling with CFSE and delivery (i.v.) to recipient mice (**Fig. 4D**). First, we determined that splenic RPM abundance was not different between WT and $Fpr2^{-/-}$ mice (**Fig. 4E**). We then quantified the abundance of $CFSE^+$ RPM in spleens of WT and $Fpr2^{-/-}$ mice 1 hour after administration of oxidized (Ox) or control (Ctrl) RBCs (**Fig. 4F-H**). When unstressed Ctrl RBCs were delivered, we found that only a small percentage of RPM were $CFSE^+$, indicating a minimal amount of erythrophagocytosis of the exogenous cells. Further, there was no difference in $CFSE^+$ RPM in $Fpr2^{-/-}$ mice compared with WT after Ctrl RBCs were administered. However, in mice given oxidized RBCs, we detected a sharp increase in the amount of $CFSE^+$ RPM indicating a robust removal of damaged RBCs from circulation. Interestingly, when we compared the extent of Ox RBC uptake by RPM between genotypes, we noted a

striking decrease in both the percentage of RPM that was $CFSE^+$ and the RPM CFSE fluorescence in *Fpr2*$^{-/-}$ mice (**Fig. 4H**). To determine whether this defect was due specifically to the lack of ALX/FPR2 signaling on macrophages, we first assessed RBC uptake in isolated primary splenocytes *ex vivo*. Spleens from WT and *Fpr2*$^{-/-}$ mice were harvested and processed into single-cell suspensions and the resulting splenocytes were then incubated with oxidatively damaged, CFSE-labeled RBCs (**Fig. 4I**). We found that RPM isolated from *Fpr2*$^{-/-}$ mice displayed decreased uptake of oxidized RBC compared with those from WT mice (**Fig. 4J**), largely recapitulating our *in vivo* observations. Finally, to establish cell specificity *in vivo*, we performed *in vivo* RBC splenic disposal assay using mice with myeloid-specific deletion of *FPR2* (h*FPR2*^{MKO}) (**Fig. 4K**). As described previously[21], these mice were generated by crossing humanized ALX/FPR2-GFP knockin floxed mice with lysozyme M-Cre expressing mice. Validation of the loss of ALX/FPR2 expression in peripheral blood leukocytes is shown in **Supplementary Fig. 4**. Interestingly, we found that while h*FPR2*^{MKO} displayed a similar amount of $CFSE^+$ RPM compared with floxed controls (h*FPR2*$^{fl/fl}$), the fluorescence intensity of CFSE within these cells was significantly lower (**Fig. 4L,M**). These results would suggest that when *FPR2* is absent from myeloid cells, engulfment of damaged RBC may not be significantly affected but rather the capacity and efficiency of processing ingested RBC cargo is acutely impacted.

Taken together, these data indicate that signaling via ALX/FPR2 specifically on RPM is critical for maintaining a healthy circulating erythroid pool. Given the importance of the receptor on this process, we next questioned whether abundance of ALX/FPR2 ligands changes during erythrophagocytosis.

3.5 Heightened erythrophagocytosis stimulates LXA_4 production

To test whether ALX/FPR2 ligand abundance is altered during RBC disposal, we performed targeted LC-MS/MS lipidomic profiling spanning the arachidonic acid (AA), docosahexaenoic acid (DHA), and eicosapentaenoic acid (EPA) metabolomes. Spleens of WT mice were collected 1 hour after mice were administered RBCs that had either been subjected to the previously described *ex vivo* oxidation of RBC or incubated with a CD47 blocking antibody (CD47 Ab RBC) (**Fig. 5A,B**). Both RBC treatments led to a clear and marked appearance of $CFSE^+$ cells in the spleen (**Fig. 5C,D**; **Supplementary Fig. 5**). Lipidomic analysis of spleens following Ox RBC challenge demonstrated a clear grouping and separation of samples based on treatment as determined by partial least squares discriminant analysis (PLS-DA), indicating a shift in global lipid mediator profiles (**Fig. 5E**). To determine the specific lipid mediators driving group separation, we performed volcano and variable importance plot analyses (**Fig. 5F,G**). These analyses revealed that nearly all the compounds that were different between treatments were upregulated, spanned each of the parent PUFA metabolomes, and included multiple families of lipid mediators (e.g., lipoxins, resolvins, prostaglandins; representative mass chromatograms of significantly changed lipid mediators are shown in **Supplementary Figures 6 and 7**). Strikingly, however, the most significantly upregulated compound in the analysis was LXA_4. Similarly, when CD47 Ab RBCs were delivered we found a similar sample grouping by PLS-DA (**Fig. 5H**) and LXA_4 was among the most upregulated lipid species in the analysis (**Fig. 5I,J**). Absolute quantification of LXA_4 and its parent PUFA (AA) confirmed an activation of the lipoxin biosynthetic pathway in both models, albeit with an amplified response after Ox RBC delivery compared with CD47

Ab incubation (**Fig. 5K**). Additionally, levels of 15-HETE were also elevated; however, due to the chromatographic conditions used, we were unable to distinguish between the 15(*R*)- and 15(*S*)- isomers. While 15(*S*)-HETE is a known intermediate in the enzymatic biosynthesis of LXA_4, we cannot definitively attribute the increase in 15-HETE to the 15(*S*)- isomer, alone. These results combined with those from *Fpr2*$^{-/-}$ mice demonstrate that splenic LXA_4 production is enhanced during induced erythrophagocytosis and its actions are required for optimal RPM uptake and disposal of damaged RBCs.

3.6 LXA_4 increases RBC uptake in macrophages *in vitro*

To determine whether LXA_4 directly targets macrophage-mediated uptake of RBCs, we employed an *in vitro* approach of differentiating RPM-like cells from isolated murine bone marrow (BM) cells (**Fig. 6A**). After stimulation with interleukin-33 and hemin, inducible RPM (iRPM) are enriched in genes characteristic of splenic RPM—mirroring what we measured in *in vivo* sorted RPM in **Fig. 4B**—compared to bone marrow-derived macrophages (BMDM; **Fig. 6B**). Importantly, while iRPM exhibit functional similarities with splenic RPM in their capacity to phagocytose RBCs, they do not completely recapitulate the phenotype observed *in vivo*. We determined that iRPM express *Fpr2* similarly to BMDM but had decreased expression of *Alox15* (**Fig. 6C**), partially mirroring what we measured in sorted RPM. We then pretreated iRPM with LXA_4 for 15 minutes prior to addition of CFSE-stained RBCs and found that it significantly increased their uptake as determined by $CFSE^+$ iRPM and CFSE fluorescence (**Fig. 6D**). These results suggest that LXA_4 stimulates the uptake and removal of RBCs via its cognate receptor, ALX/FPR2.

3.7 LXA_4 is critical for efficient RBC disposal by splenic RPM

Given that LXA_4 abundance was increased in the spleen during heightened RBC uptake and its exogenous administration stimulated increased RBC uptake *in vitro*, we next questioned the impact of disrupting its production on erythrophagocytosis. Using mice with genetic deletion of 12/15-lipoxygenase (*Alox15*$^{-/-}$)—a critical LXA_4 biosynthetic enzyme—we first confirmed that LXA_4 abundance in the spleen was indeed decreased (**Fig 7A**). Next, we subjected the mice to *in vivo* RBC uptake assay using Ox RBCs (**Fig. 7B**). Similar to what we observed in *Fpr2*$^{-/-}$ mice, we found that mice lacking *Alox15* had no detectable basal difference in RPM-mediated uptake of Ctrl RBCs but exhibited a significant decrease in erythrophagocytosis of damaged RBCs (**Fig. 7C,D**). To test whether exogenous LXA_4 could restore this defect, we administered LXA_4 (i.p.) to WT and *Alox15*$^{-/-}$ mice 15 minutes prior to delivery of Ox RBCs (**Fig. 7E**). Interestingly, we did not observe an LXA_4-induced enhancement of RPM uptake in WT mice, but in those lacking *Alox15*$^{-/-}$ there was an increase, restoring levels of uptake to that of WT mice (**Fig. 7F,G**). These results suggest that LXA_4 is sufficient to enhance RPM-mediated clearance of RBCs.

4. Discussion

In this study, we establish an integral role for ALX/FPR2 signaling in maintaining erythroid homeostasis. In mice lacking ALX/FPR2, we found elevated levels of aged RBCs in circulation, indicating a decreased rate of basal turnover. Histological analyses of spleens from *Fpr2*$^{-/-}$ mice showed decreased abundance of heme and iron deposits in red pulp further suggesting decreased RBC turnover, while transcriptomics revealed an altered splenic macrophage phenotype—driven in part by changes in heme metabolism. Functionally, we found that during on-demand erythrophagocytosis splenic production of LXA_4, a key proresolving ligand of ALX/FPR2, was increased in WT mice. However, in mice lacking ALX/FPR2 or the biosynthetic enzyme critical for LXA_4 production (i.e., 12/15-LOX), erythrophagocytosis was impaired. Critically, myeloid-specific deletion of *FPR2* also impaired efficient splenic erythrophagocytosis. Finally, when administered exogenous LXA_4, the deficient erythrophagocytosis of *Alox15*$^{-/-}$ mice was restored. Together, these results indicate that in response to RBC stress splenic LXA_4 production is enhanced, activating ALX/FPR2 on red pulp macrophages to promote erythrophagocytosis and removal of dysfunctional erythrocytes from circulation to maintain hematologic homeostasis.

The findings presented here offer new insights into the mechanisms of local proresolving signaling pathways significantly impacting systemic immune processes. By acting locally on macrophages in the spleen LXA_4-ALX/FPR2 signaling is necessary to preserve an optimal population of circulating erythrocytes while it is also sufficient to overcome acute erythroid stress. The ability to influence the RBC pool is critical as small

variations in the fitness of erythrocytes can have profound physiological and immunological effects.[27,28] As RBCs age or are stressed they undergo a variety of alterations including modifications in metabolism, morphology, and membrane structure which result in functional decline characterized by decreased ability to facilitate gas exchange and an increased risk of aggregation.[29-31] Additionally, recent reports have suggested that RBCs also have a direct immunomodulatory impact via their ability to bind and deliver inflammatory agonists like cytokines and nucleic acids, stimulating innate immune responses.[32,33] Thus, preserving a healthy pool of circulating RBCs is important in mediating the risks of infection, anemia, and thrombosis, and is critical in the body's response to malaria and sickle cell disease.

Recently it was demonstrated that targeting the ALX/FPR2 receptor with proresolving ligands during sickle cell crisis may be a beneficial treatment strategy as mice exhibited ameliorated cerebral thrombosis[34] and vaso-occlusive pathologies.[22] While the importance of ALX/FPR2 in the development and progression of cardiovascular diseases, like atherosclerosis,[35] aortic aneurysm,[36,37] heart failure,[38-40] and infection-induced cardiac dysfunction[41,42] has been well-documented, its role in hematologic pathologies remains comparatively unexplored.

Results of our study complement and extend previous work that has established a role for proresolving lipid mediators in erythrocyte uptake and disposal[22,23,43-46] by demonstrating the myeloid dependence of ALX/FPR2 signaling on the process. These

previous reports found that the abundance of SPM, including ALX/FPR2 ligands, are decreased in spleens of mice with sickle cell disease and demonstrate the ability of D- and E-series resolvins, as well as the recently described cysteinyl-resolvins, to promote macrophage uptake of senescent RBCs *in vivo* and *in vitro*. However, the impact of LXA_4, specifically, has not been described nor has the essential role of ALX/FPR2. In our models of induced erythrophagocytosis we found that the abundance of SPM species in spleen were broadly increased, with LXA_4 the most significantly induced mediator. In addition to LXA4, we found that levels of RvD4, 17*R*-RvD3, Maresin 1, RvE2, and RvE4 were increased after Ox RBC challenge. RvE4 has previously been shown to be biosynthesized during co-incubation of human RBCs and macrophages, and stimulation with RvE4 potently enhanced erythrophagocytosis in human macrophages.[44] We also detected an increased abundance of 17*R*-RvD3. This is notable as the related mediator and ALX/FPR2 ligand, 17*R*-RvD1, was previously found to be decreased in spleens of sickle cell mice and its administration was sufficient to enhance splenic RBC disposal[22] and, more recently to improve cardiomyopathy in humanized sickle cell mice.[47] Though we did not identify 17*R*-RvD1, both mediators are derived from the aspirin- or COX-2-dependent conversion of DHA but differ in their subsequent biosynthetic routes and epoxide intermediates. While it is not clear that 17*R*-RvD3 can bind and activate ALX/FPR2, its epimer, RvD3, is a known ligand of the receptor.[48,49]

Importantly, much of the previous work referenced above was conducted in a humanized mouse model of sickle cell anemia. It has been demonstrated that while

these mice share important phenotypic similarities with sickle cell diseases patients, they also display marked changes in splenic morphology, particularly related to the red pulp.[50] Conversely, the current study was performed in healthy mice with no overt splenic morbidity. Thus, the results presented here demonstrate the critical importance of this signaling pathway to basal splenic erythrocyte processing and maintenance of hemodynamic homeostasis.

The current study provides new mechanistic insight into the role of ALX/FPR2 in erythroid homeostasis. For the first time, we have demonstrated a macrophage-intrinsic defect in erythrophagocytosis in the absence of ALX/FPR2 signaling, using both isolated primary RPM and mice with myeloid-specific deletion of the receptor. Interestingly, comparing the impact of global and myeloid-specific knockout of *Fpr2* revealed a divergence in erythrophagocytic function. While RPM from myeloid-deficient mice could recognize and engulf damaged RBCs similarly to floxed controls, their reduced fluorescence intensity indicated a lower RBC load per cell. This suggests that without ALX/FPR2, RPM may become functionally satiated more quickly, with impaired capacity for simultaneous degradation of multiple RBCs. Additionally, RNA-sequencing from *Fpr2*$^{-/-}$ isolated splenic macrophages revealed significant changes in heme metabolism pathways, pointing to a potential defect in processing of RBC-derived heme. Although the mechanism for this reduced RBC processing remains unclear, it may involve intermediary metabolism, which is increasingly recognized as essential for macrophages to degrade multiple apoptotic cells.[51-53] Indeed, we have previously shown that ALX/FPR2 activation promotes mitochondrial metabolism and efferocytosis

via AMPK-dependent signaling.[54-56] Additionally, given that RBC digestion releases significant quantities of reactive species (i.e., heme, iron), ALX/FPR2-mediated suppression of ROS production may help RPM adapt during high-demand erythrophagocytic conditions. This aligns with recent reports demonstrating that ALX/FPR2 activation protects against macrophages ferroptosis.[36,57] While our findings establish a functional role for the LXA_4–ALX/FPR2 signaling axis in enhancing splenic erythrophagocytosis, further studies are needed to more fully elucidate the underlying mechanisms.

Overall, our findings reveal new functions of the LXA_4-ALX/FPR2 signaling axis and contribute to a growing body of literature assigning importance to lipid mediators in the uptake and disposal of aged or damaged erythrocytes. These findings offer an additional physiologic mechanism that may bolster the capability of ALX/FPR2 activation to combat systemic unresolved inflammation and inform the development of new therapeutic approaches to target the pathway during transfusion-related immunomodulation or acute hemolytic crises.

5. References

1. Klei TR, Meinderts SM, van den Berg TK, et al. From the Cradle to the Grave: The Role of Macrophages in Erythropoiesis and Erythrophagocytosis. Front Immunol. 2017;8:73.
2. Neri S, Swinkels DW, Matlung HL, et al. Novel concepts in red blood cell clearance. Curr Opin Hematol. 2021;28(6):438-444.
3. Slusarczyk P, Mleczko-Sanecka K. The Multiple Facets of Iron Recycling. Genes (Basel). 2021;12(9):1364.
4. Muckenthaler MU, Rivella S, Hentze MW, et al. A Red Carpet for Iron Metabolism. Cell. 2017;168(3):344-361.
5. Hod EA, Zhang N, Sokol SA, et al. Transfusion of red blood cells after prolonged storage produces harmful effects that are mediated by iron and inflammation. Blood. 2010;115(21):4284-4292.
6. Youssef LA, Rebbaa A, Pampou S, et al. Increased erythrophagocytosis induces ferroptosis in red pulp macrophages in a mouse model of transfusion. Blood. 2018;131(23):2581-2593.
7. Woodruff AW, Ansdell VE & Pettitt LE. Cause of anaemia in malaria. Lancet. 1979;1(8125):1055-1057.
8. Michel M, Crickx E, Fattizzo B, et al. Autoimmune haemolytic anaemias. Nat Rev Dis Primers. 2024;10(1):82.
9. Costea N. The differential diagnosis of hemolytic anemias. Med Clin North Am. 1973;57(2):289-302.
10. Serhan CN. Pro-resolving lipid mediators are leads for resolution physiology. Nature. 2014;510(7503):92-101.
11. Serhan CN, Levy BD. Resolvins in inflammation: emergence of the pro-resolving superfamily of mediators. J Clin Invest. 2018;128(7):2657-2669.
12. Decker C, Sadhu S, Fredman G. Pro-Resolving Ligands Orchestrate Phagocytosis. Front Immunol. 2021;12:660865.
13. Chiang N, Arita M, Serhan CN. Anti-inflammatory circuitry: lipoxin, aspirin-triggered lipoxins and their receptor ALX. Prostaglandins Leukot Essent Fatty Acids. 2005;73(3-4):163-177.
14. Maderna P, Cottell DC, Toivonen T, et al. FPR2/ALX receptor expression and internalization are critical for lipoxin A4 and annexin-derived peptide-stimulated phagocytosis. FASEB J. 2010;24(11):4240-4249.
15. Fiore S, Maddox JF, Perez HD, et al. Identification of a human cDNA encoding a functional high affinity lipoxin A4 receptor. J Exp Med. 1994;180(1):253-260.
16. Krishnamoorthy S, Recchiuti A, Chiang N, et al. Resolvin D1 binds human phagocytes with evidence for proresolving receptors. Proc Natl Acad Sci U S A. 2010;107(4):1660-1665.
17. Sansbury BE, Spite M. Resolution of Acute Inflammation and the Role of Resolvins in Immunity, Thrombosis, and Vascular Biology. Circ Res. 2016;119(1):113-130.
18. Fredman G, Serhan CN. Specialized pro-resolving mediators in vascular inflammation and atherosclerotic cardiovascular disease. Nat Rev Cardiol. 2024;21(11):808-823.
19. Giannakis N, Sansbury BE, Patsalos A, et al. Dynamic changes to lipid mediators support transitions among macrophage subtypes during muscle regeneration. Nat Immunol. 2019;20(5):626-636.
20. Hellmann J, Sansbury BE, Wong B, et al. Biosynthesis of D-Series Resolvins in Skin Provides Insights into their Role in Tissue Repair. J Invest Dermatol. 2018;138(9):2051-2060.
21. Sansbury BE, Li X, Wong B, et al. Myeloid ALX/FPR2 regulates vascularization following tissue injury. Proc Natl Acad Sci U S A. 2020;117(25):14354-14364.

22. Matte A, Recchiuti A, Federti E, et al. Resolution of sickle cell disease-associated inflammation and tissue damage with 17R-resolvin D1. Blood. 2019;133(3):252-265.
23. Norris PC, Libreros S, Serhan CN. Resolution metabolomes activated by hypoxic environment. Sci Adv. 2019;5(10):eaax4895.
24. Saxena RK, Bhardwaj N, Sachar S, et al. A Double in vivo Biotinylation Technique for Objective Assessment of Aging and Clearance of Mouse Erythrocytes in Blood Circulation. Transfus Med Hemother. 2012;39(5):335-341.
25. Oldenborg PA, Zheleznyak A, Fang YF, et al. Role of CD47 as a marker of self on red blood cells. Science. 2000;288(5473):2051-2054.
26. Kohyama M, Ise W, Edelson BT, et al. Role for Spi-C in the development of red pulp macrophages and splenic iron homeostasis. Nature. 2009;457(7227):318-321.
27. Dobkin J, Mangalmurti NS. Immunomodulatory roles of red blood cells. Curr Opin Hematol. 2022;29(6):306-309.
28. Niu C, Zhang J. Immunoregulation role of the erythroid cells. Front Immunol. 2024;15:1466669.
29. Bosch FH, Werre JM, Schipper L, et al. Determinants of red blood cell deformability in relation to cell age. Eur J Haematol. 1994;52(1):35-41.
30. Mohanty JG, Nagababu E, Rifkind JM. Red blood cell oxidative stress impairs oxygen delivery and induces red blood cell aging. Front Physiol. 2014;5:84.
31. Weisel JW, Litvinov RI. Red blood cells: the forgotten player in hemostasis and thrombosis. J Thromb Haemost. 2019;17(2):271-282.
32. Karsten E, Breen E, Herbert BR. Red blood cells are dynamic reservoirs of cytokines. Sci Rep. 2018;8(1):3101.
33. Lam LKM, Murphy S, Kokkinaki D, et al. DNA binding to TLR9 expressed by red blood cells promotes innate immune activation and anemia. Sci Transl Med. 2021;13(616):eabj1008.
34. Ansari J, Senchenkova EY, Vital SA, et al. Targeting the AnxA1/Fpr2/ALX pathway regulates neutrophil function, promoting thromboinflammation resolution in sickle cell disease. Blood. 2021;137(11):1538-1549.
35. Drechsler M, de Jong R, Rossaint J, et al. Annexin A1 counteracts chemokine-induced arterial myeloid cell recruitment. Circ Res. 2015;116(5):827-835.
36. Filiberto AC, Ladd Z, Leroy V, et al. Resolution of inflammation via RvD1/FPR2 signaling mitigates Nox2 activation and ferroptosis of macrophages in experimental abdominal aortic aneurysms. FASEB J. 2022;36(11):e22579.
37. Petri MH, Thul S, Andonova T, et al. Resolution of Inflammation Through the Lipoxin and ALX/FPR2 Receptor Pathway Protects Against Abdominal Aortic Aneurysms. JACC Basic Transl Sci. 2018;3(6):719-727.
38. Garcia RA, Lupisella JA, Ito BR, et al. Selective FPR2 Agonism Promotes a Proresolution Macrophage Phenotype and Improves Cardiac Structure-Function Post Myocardial Infarction. JACC Basic Transl Sci. 2021;6(8):676-689.
39. Kain V, Ingle KA, Colas RA, et al. Resolvin D1 activates the inflammation resolving response at splenic and ventricular site following myocardial infarction leading to improved ventricular function. J Mol Cell Cardiol. 2015;84:24-35.
40. Kain V, Liu F, Kozlovskaya V, et al. Resolution Agonist 15-epi-Lipoxin A(4) Programs Early Activation of Resolving Phase in Post-Myocardial Infarction Healing. Sci Rep. 2017;7(1):9999.
41. Chen J, Austin-Williams S, O'Riordan CE, et al. Formyl Peptide Receptor Type 2 Deficiency in Myeloid Cells Amplifies Sepsis-Induced Cardiac Dysfunction. J Innate Immun. 2023;15(1):548-561.

42. das Dores Pereira R, Rabelo RAN, Leite PG, et al. Role of formyl peptide receptor 2 (FPR2) in modulating immune response and heart inflammation in an experimental model of acute and chronic Chagas disease. Cell Immunol. 2021;369:104427.
43. Nshimiyimana R, Libreros S, Simard M, et al. Stereochemistry and functions of the new cysteinyl-resolvin, 4S,5R-RCTR1, in efferocytosis and erythrophagocytosis of human senescent erythrocytes. Am J Hematol. 2023;98(7):1000-1016.
44. Reinertsen AF, Libreros S, Nshimiyimana R, et al. Metabolization of Resolvin E4 by omega-Oxidation in Human Neutrophils: Synthesis and Biological Evaluation of 20-Hydroxy-Resolvin E4 (20-OH-RvE4). ACS Pharmacol Transl Sci. 2023;6(12):1898-1908.
45. Libreros S, Shay AE, Nshimiyimana R, et al. A New E-Series Resolvin: RvE4 Stereochemistry and Function in Efferocytosis of Inflammation-Resolution. Front Immunol. 2020;11:631319.
46. Simard M, Nshimiyimana R, Chiang N, et al. A potent proresolving mediator 17R-resolvin D2 from human macrophages, monocytes, and saliva. Sci Adv. 2024;10(47):eadq4785.
47. Federti E, Mattoscio D, Recchiuti A, et al. 17(R)-Resolvin D1 protects against sickle cell-related inflammatory cardiomyopathy in humanized mice. Blood. 2025;145(17):1915-1928.
48. Arnardottir HH, Dalli J, Norling LV, et al. Resolvin D3 Is Dysregulated in Arthritis and Reduces Arthritic Inflammation. J Immunol. 2016;197(6):2362-2368.
49. Dalli J, Winkler JW, Colas RA, et al. Resolvin D3 and aspirin-triggered resolvin D3 are potent immunoresolvents. Chem Biol. 2013;20(2):188-201.
50. Kamimura S, Smith M, Vogel S, et al. Mouse models of sickle cell disease: Imperfect and yet very informative. Blood Cells Mol Dis. 2024;104:102776.
51. Schilperoort M, Ngai D, Sukka SR, et al. The role of efferocytosis-fueled macrophage metabolism in the resolution of inflammation. Immunol Rev. 2023;319(1):65-80.
52. Yurdagul A, Jr., Subramanian M, Wang X, et al. Macrophage Metabolism of Apoptotic Cell-Derived Arginine Promotes Continual Efferocytosis and Resolution of Injury. Cell Metab. 2020;31(3):518-533.e10.
53. Zhang S, Weinberg S, DeBerge M, et al. Efferocytosis Fuels Requirements of Fatty Acid Oxidation and the Electron Transport Chain to Polarize Macrophages for Tissue Repair. Cell Metab. 2019;29(2):443-456.e5.
54. Calderin EP, Zheng JJ, Boyd NL, et al. Exercise-induced specialized proresolving mediators stimulate AMPK phosphorylation to promote mitochondrial respiration in macrophages. Mol Metab. 2022;66:101637.
55. Hosseini Z, Marinello M, Decker C, et al. Resolvin D1 Enhances Necroptotic Cell Clearance Through Promoting Macrophage Fatty Acid Oxidation and Oxidative Phosphorylation. Arterioscler Thromb Vasc Biol. 2021;41(3):1062-1075.
56. Pena Calderin E, Zheng JJ, Boyd NL, et al. Exercise-Stimulated Resolvin Biosynthesis in the Adipose Tissue Is Abrogated by High-Fat Diet-Induced Adrenergic Deficiency. Arterioscler Thromb Vasc Biol. 2025;45(7):1090-1110.
57. Li X, Xu H, Liu K, et al. LXA4 alleviates inflammation and ferroptosis in cigarette smoke induced chronic obstructive pulmonary disease via the ALX/FPR2 receptor. Int Immunopharmacol. 2025;151:114322.

6. Figure Legends

Figure 1. Deletion of ALX/FPR2 receptor disrupts RBC turnover. The basal rate of RBC turnover in wild type (WT) mice and mice lacking the ALX/FPR2 receptor (*Fpr2*$^{-/-}$) was determined by a two-step biotinylation assay. (A) Representative flow cytometry dot plots are shown. Circulating RBCs (Ter119^{+}) were gated based on biotin positivity. (B) Quantification of each RBC population is shown over time. (C) Representative flow cytometry histogram and quantification of CD47 expression on circulating RBCs. (D) Representative flow cytometry dot plots and quantification of circulating reticulocytes (Retic; CD71^{+}Ter119^{+}). Data are mean ± SEM. *p<0.05, **p<0.01, ***p<0.001 as determined by two-way ANOVA or unpaired Student's t-test.

Figure 2. Decreased markers of erythrophagocytosis in spleens of *Fpr2*$^{-/-}$ mice. (A) Representative images of H&E-stained spleen sections. Arrows indicate areas with heme deposits. Quantification of the ratio of red pulp to white pulp area (B) and heme deposits (C) as determined from H&E sections. Representative images (D) and quantification (E) of Prussian blue-stained spleen sections. (F) Representative images of F4/80-stained spleen sections. (G) Quantification of total spleen heme as determined by colorimetric biochemical assay. (A,D,F) Dashed boxes on images indicate areas of red pulp that are displayed at higher magnification. Scale bars: 500 μm in unmagnified and 30 μm in magnified images. Data are mean ± SEM. n = 3-4 per group. *p<0.05, **p<0.01, as determined by unpaired Student's t-test.

Figure 3. *Fpr2*$^{-/-}$ mice have altered splenic transcriptome with particular effects on splenic macrophages. Schematic of spleens (A) or isolated F4/80^{+} splenocytes (D) from WT and *Fpr2*$^{-/-}$ mice subjected to RNA-sequencing. (B,E) Volcano plot analyses of differentially expressed genes (DEG) in *Fpr2*$^{-/-}$ mice compared with WT. Downregulated genes are shown in blue; upregulated in red. (C,F) Gene ontology (GO): biological processes enrichment analyses of DEG displayed with related pathways grouped into functional clusters. (G) The change in expression of the component DEG contained in the GO pathways is shown for *Fpr2*$^{-/-}$ F4/80^{+} splenocytes. An accompanying heatmap illustrates the corresponding functional clusters for each DEG. n = 3–4 spleens per genotype; 5 F4/80^{+} splenocyte samples per genotype.

Figure 4. ALX/FPR2 deletion impairs splenic macrophage uptake of damaged RBCs. (A) Schematic of *Spic*-EGFP reporter mouse. (B,C) Gene expression of flow cytometry-sorted splenocytes from *Spic*-EGFP mice. (D) Schematic of *in vivo* RBC uptake assay in WT and *Fpr2*$^{-/-}$ mice. (E) Representative flow cytometry dot plot of splenic red pulp macrophages (RPM) identification and quantification. (F,G) Representative flow cytometry dot plots and overlaid histograms of RPM in WT and *Fpr2*$^{-/-}$ mice 1h after administration of untreated (Ctrl) or oxidized (Ox) RBCs. (H) Quantification of CFSE^{+} RPM and RPM CFSE MFI. (I) Primary splenic RPM from WT and *Fpr2*$^{-/-}$ were isolated and incubated *ex vivo* with Ox RBCs for 1h. Representative flow cytometry dot plots and overlaid histograms are shown. (J) Quantification of CFSE^{+} RPM and RPM CFSE MFI. (K) Schematic of *in vivo* RBC uptake assay in humanized *FPR2* floxed mice (h*FPR2*$^{fl/fl}$) and mice with myeloid specific deletion of h*FPR2*

(h*FPR2*^{MKO}). (L) Representative flow cytometry dot plots and quantification of CFSE^{+} RPM and (M) representative flow cytometry overlaid histograms and quantification of RPM CFSE MFI 1h after administration Ox RBCs. Data are mean ± SEM. n = 4 per group (B,C), 5–7 per group (E,H), 5–9 per group (J), 6 per group (K,L). **p<0.01, ***p<0.001, ****p<0.0001 as determined by unpaired Student's t-test (B,C,E,J,K,L) or two-way ANOVA (H).

Figure 5. Lipoxin A_4 (LXA_4) is increased during splenic uptake of damaged RBCs. Schematic of *in vivo* uptake assays in which RBCs were oxidized (Ox RBC; A) or incubated with CD47 blocking antibody (Ab) or IgG control antibody (IgG; B) *ex vivo* prior to administration (via retroorbital injection). Spleens were removed 1h later and subjected to flow cytometric (C,D) or targeted LC-MS/MS lipidomic analyses (E-K). (C,D) Representative flow cytometric dot plots showing CFSE^{+} cells in spleen. (E,H) PLS-DA two-dimensional scores plot showing clustering of samples based on their global lipidomic profiles. Volcano plot (F,I) and variable importance plot (VIP; G,J) analyses displaying significantly changed lipid mediators colored according to their parent fatty acid (orange – Arachidonic Acid; blue – Docosahexaenoic Acid; green – Eicosapentaenoic Acid; purple – Docosapentaenoic Acid). (K) Absolute abundance of selected Arachidonic Acid (AA)-derived lipid mediators. Data are mean ± SEM. n = 4 per group (Ctrl vs. Ox RBC); 5 per group (IgG vs. CD47 Ab RBC). *p<0.05 as determined by unpaired Student's t-test vs. appropriate control group.

Figure 6. LXA_4 stimulates macrophage uptake of RBCs. (A) Schematic of *in vitro* generation of induced RPM (iRPM) from bone marrow (BM) cells using macrophage colony-stimulating factor (M-CSF), interleukin-33 (IL-33), and hemin. (B,C) Gene expression in iRPM and bone marrow-derived macrophages (BMDM). (D) Representative flow cytometry dot plots, overlaid histograms, and quantification of iRPM following 15 min stimulation with LXA_4 prior to addition of CFSE-stained RBCs. Data are mean ± SEM. n = 3 (B,C) or 4 independent experiments including at least 3 technical replicates per experiment (D). *p<0.05 as determined by unpaired Student's t-test.

Figure 7. LXA_4 is sufficient to rescue defective erythrophagocytosis. (A) LXA_4 abundance in spleens of WT and 12/15-lipoxygenase deficient mice (*Alox15*$^{-/-}$). (B) Schematic of *in vivo* RBC uptake assay in WT and *Alox15*$^{-/-}$ mice. (C,D) Representative flow cytometry dot plots and quantification of $CFSE^+$ splenic RPM in WT and *Alox15*$^{-/-}$ mice 1h after administration of untreated (Ctrl) or oxidized (Ox) RBCs. (E) Schematic of *in vivo* uptake assay where WT and *Alox15*$^{-/-}$ received exogenous LXA_4 or vehicle (Veh) 15 min prior to Ox RBC administration. (F) Representative flow cytometry dot plots and overlaid histograms of RPM from *Alox15*$^{-/-}$ mice following vehicle (Veh) or LXA_4 treatment and Ox RBC administration. (G) Quantification of $CFSE^+$ RPM (%) and RPM CFSE MFI. Data are mean ± SEM. n = 4-7 per group (A), 4 per group (D), or 7–8 per group (G). *p<0.05, **p<0.01 as determined by unpaired Student's t-test (A) or two-way ANOVA (D,G).

Figure 1

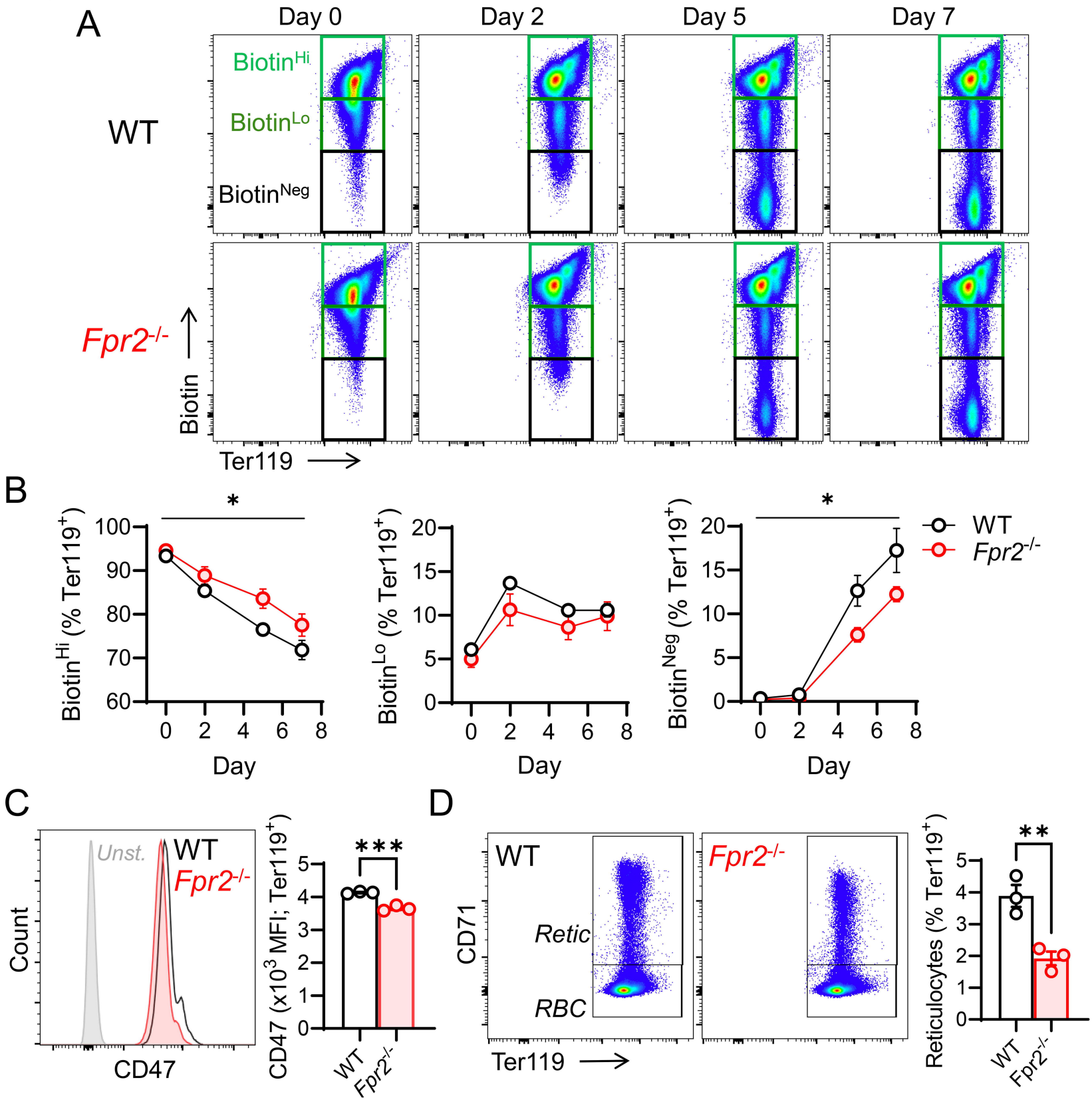
A
Day 0
Day 2
Day 5
Day 7
WT
Fpr2-/-
BiotinHi
BiotinLo
BiotinNeg
Biotin
Ter119
B
BiotinHi (% Ter119+)
BiotinLo (% Ter119+)
BiotinNeg (% Ter119+)
Day
WT
Fpr2-/-
C
Unst.
WT
Fpr2-/-
Count
CD47
CD47 (x10^3 MFI; Ter119+)
D
WT
Fpr2-/-
Retic
RBC
CD71
Ter119
Reticulocytes (% Ter119+)

Figure 2

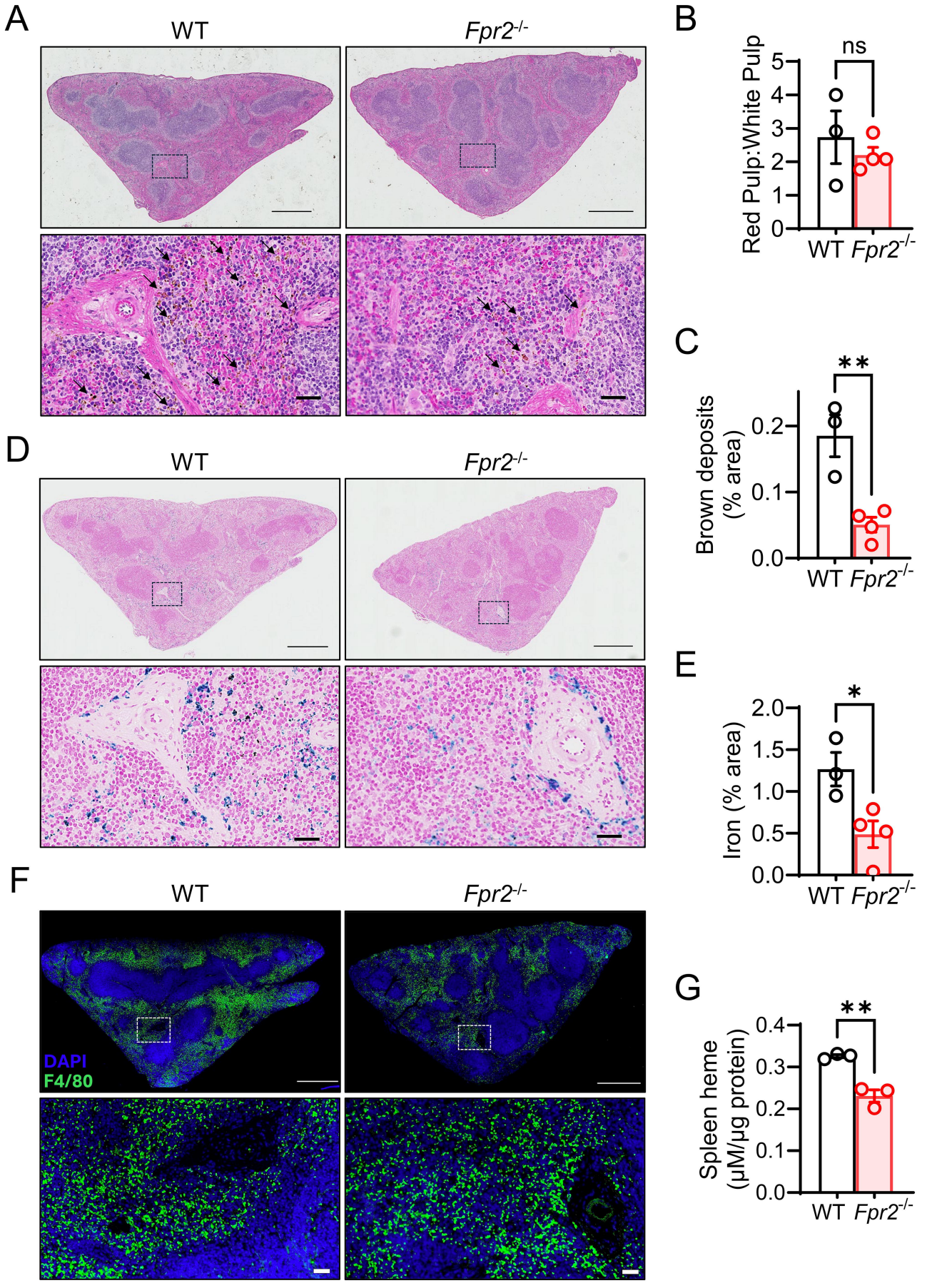
A
WT
Fpr2-/-
B
Red Pulp:White Pulp
ns
WT
Fpr2-/-
C
Brown deposits (% area)
**
WT
Fpr2-/-
D
WT
Fpr2-/-
E
Iron (% area)
*
WT
Fpr2-/-
F
WT
Fpr2-/-
DAPI
F4/80
G
Spleen heme (μM/μg protein)
**
WT
Fpr2-/-

Figure 3

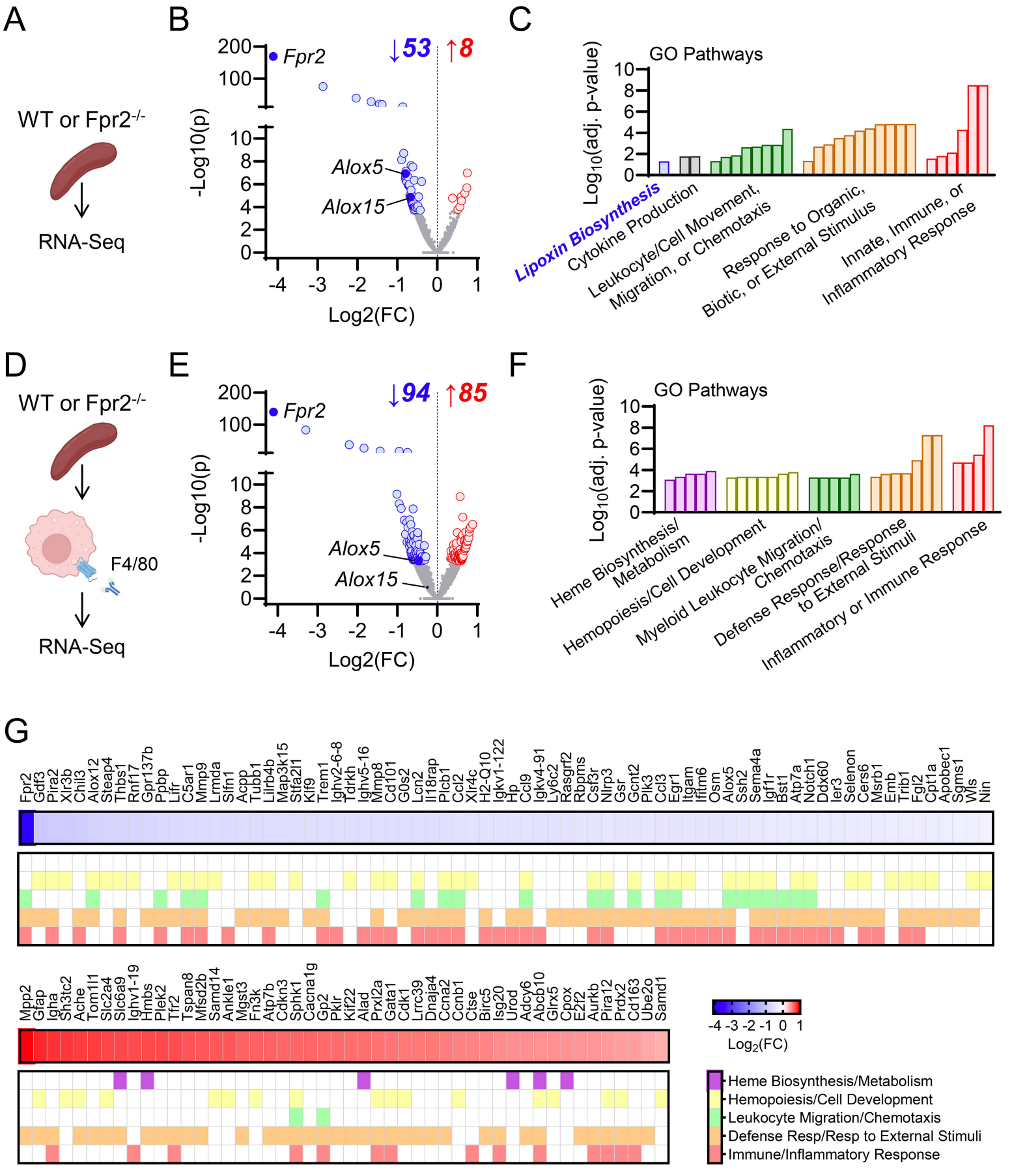
A
WT or Fpr2-/-
RNA-Seq
B
Fpr2
↓53
↑8
Alox5
Alox15
-Log10(p)
Log2(FC)
C
GO Pathways
Log10(adj. p-value)
Lipoxin Biosynthesis
Cytokine Production
Leukocyte/Cell Movement, Migration, or Chemotaxis
Response to Organic, Biotic, or External Stimulus
Innate, Immune, or Inflammatory Response
D
WT or Fpr2-/-
F4/80
RNA-Seq
E
Fpr2
↓94
↑85
Alox5
Alox15
-Log10(p)
Log2(FC)
F
GO Pathways
Log10(adj. p-value)
Heme Biosynthesis/ Metabolism
Hemopoiesis/Cell Development
Myeloid Leukocyte Migration/ Chemotaxis
Defense Response/Response to External Stimuli
Inflammatory or Immune Response
G
Fpr2 Gdf3 Pira2 Xlr3b Chil3 Alox12 Steap4 Thbs1 Rnf17 Gpr137b Ppbp Lifr C5ar1 Mmp9 Lrmda Sifn1 Acpp Tubb1 Lilrb4b Map3k15 Stfa2l1 Klf9 Trem1 Ighv2-6-8 Tdrkh Ighv5-16 Mmp8 Cd101 G0s2 Lcn2 Il18rap Plcb1 Ccl2 Xlr4c H2-Q10 Igkv1-122 Hp Ccl9 Igkv4-91 Ly6c2 Rasgrf2 Rbpms Csf3r Nlrp3 Gsr Gcnt2 Plk3 Ccl3 Egr1 Itgam Ifitm6 Osm Alox5 Ssh2 Sema4a Igf1r Bst1 Atp7a Notch1 Ddx60 Ier3 Selenon Cers6 Msrb1 Emb Trib1 Fgl2 Cpt1a Apobec1 Sgms1 Wls Nin
Mpp2 Gfap Igha Sh3tc2 Ache Tom1l1 Slc2a4 Slc6a9 Ighv1-19 Hmbs Plek2 Tfr2 Tspan8 Mfsd2b Samd14 Ankle1 Mgst3 Fn3k Atp7b Cdkn3 Sphk1 Cacna1g Gp2 Pklr Kif22 Alad Prxl2a Gata1 Cdk1 Lrrc39 Dnaja4 Ccna2 Ccnb1 Ctse Birc5 Isg20 Urod Adcy6 Abcb10 Glrx5 Cpox E2f2 Aurkb Pira12 Prdx2 Cd163 Ube2o Samd1
-4 -3 -2 -1 0 1
Log2(FC)
Heme Biosynthesis/Metabolism
Hemopoiesis/Cell Development
Leukocyte Migration/Chemotaxis
Defense Resp/Resp to External Stimuli
Immune/Inflammatory Response

Figure 4

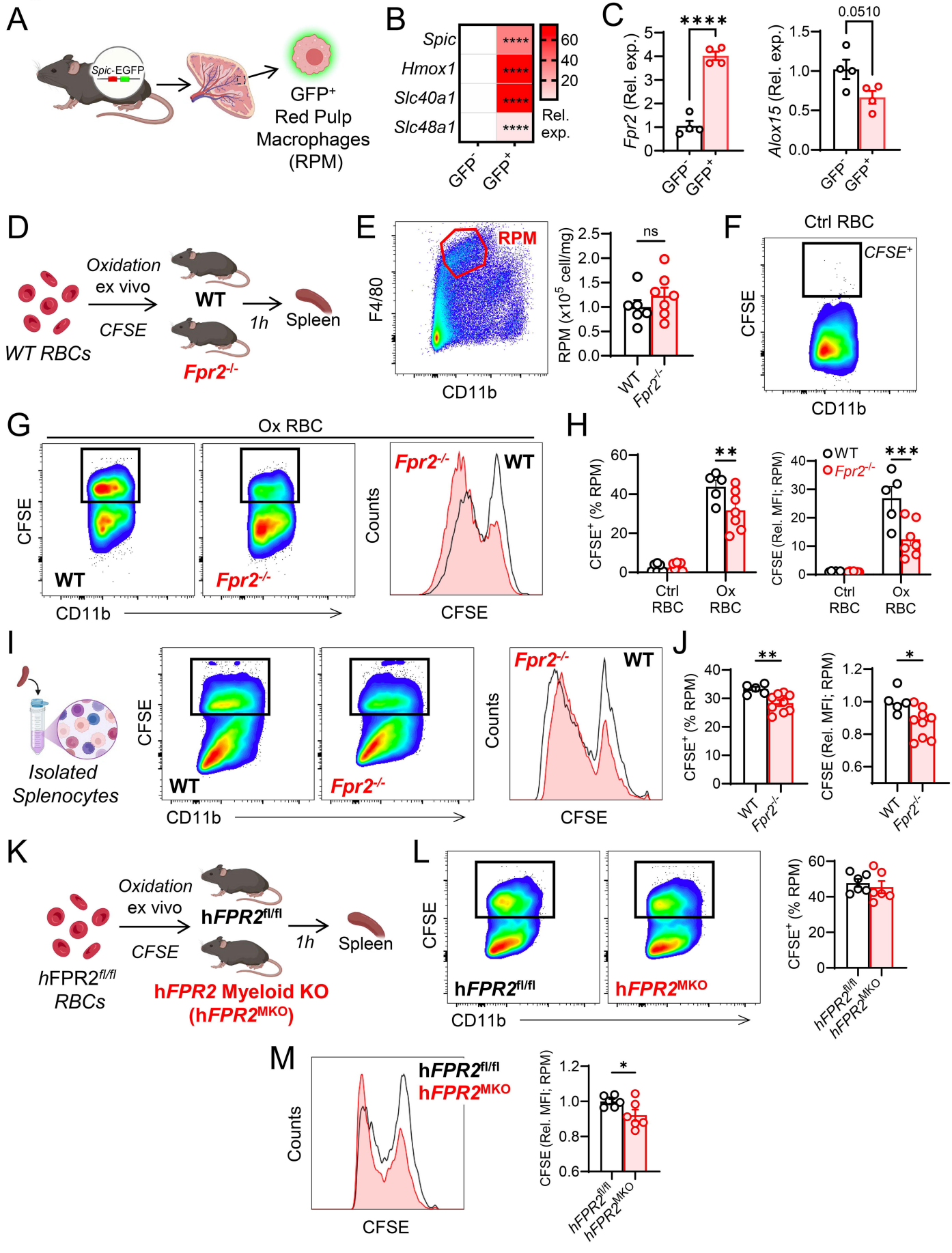
A
Spic-EGFP
GFP+ Red Pulp Macrophages (RPM)
B
Spic
Hmox1
Slc40a1
Slc48a1
****
60
40
20
Rel. exp.
GFP-
GFP+
C
Fpr2 (Rel. exp.)
Alox15 (Rel. exp.)
0.0510
D
Oxidation ex vivo
CFSE
WT RBCs
WT
Fpr2-/-
1h
Spleen
E
RPM
F4/80
CD11b
RPM (x10^5 cell/mg)
ns
F
Ctrl RBC
CFSE+
CFSE
CD11b
G
Ox RBC
CFSE
CD11b
WT
Fpr2-/-
Counts
H
CFSE+ (% RPM)
CFSE (Rel. MFI; RPM)
Ctrl RBC
Ox RBC
I
Isolated Splenocytes
J
K
hFPR2fl/fl RBCs
hFPR2 Myeloid KO (hFPR2MKO)
L
hFPR2fl/fl
hFPR2MKO
M

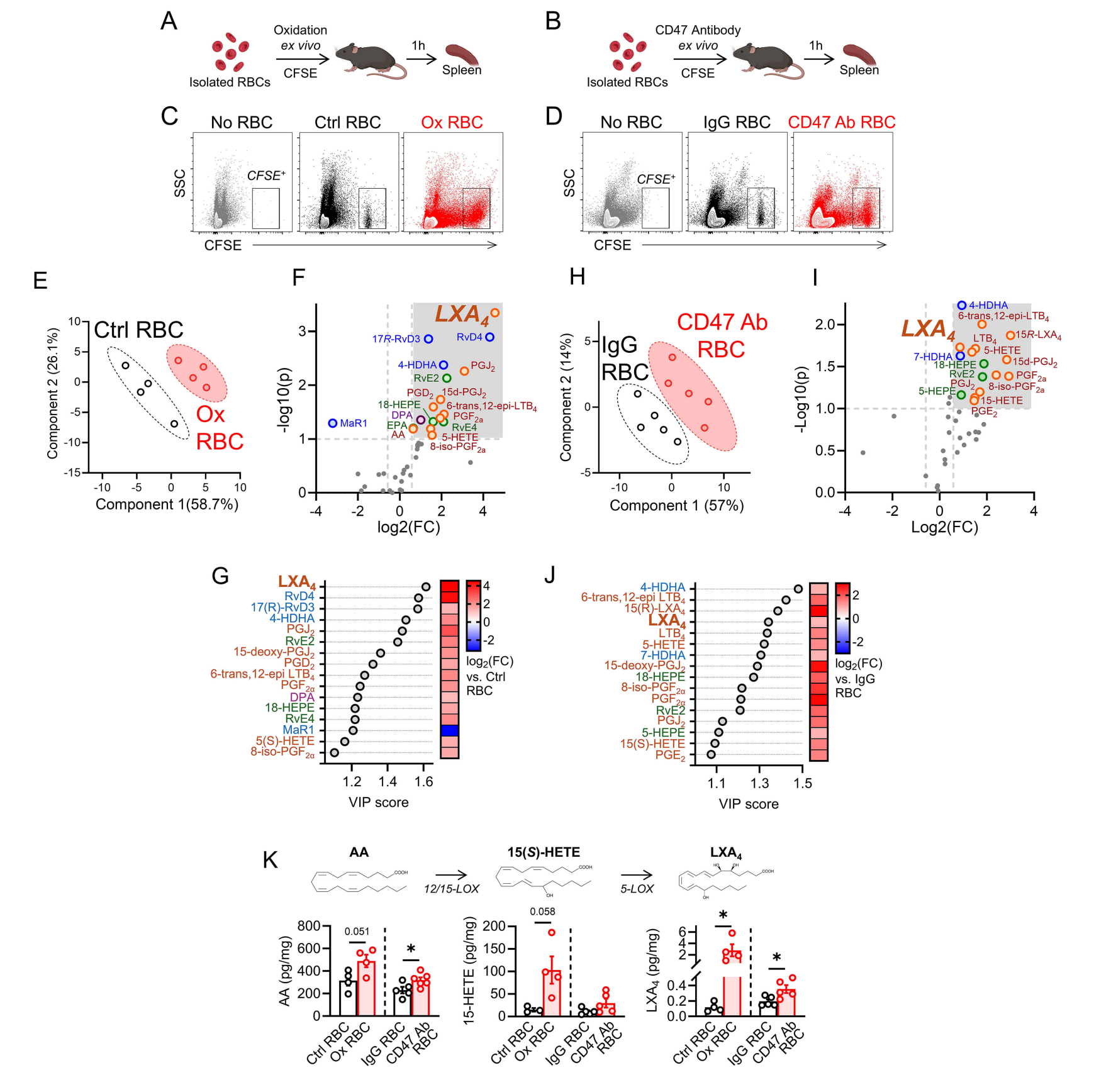
A
Oxidation
ex vivo
CFSE
1h
Isolated RBCs
Spleen
B
CD47 Antibody
ex vivo
CFSE
1h
Isolated RBCs
Spleen
C
No RBC
Ctrl RBC
Ox RBC
SSC
CFSE+
CFSE
D
No RBC
IgG RBC
CD47 Ab RBC
SSC
CFSE+
CFSE
E
Ctrl RBC
Ox RBC
Component 2 (26.1%)
Component 1(58.7%)
F
LXA4
17R-RvD3
RvD4
4-HDHA
PGJ2
RvE2
PGD2
15d-PGJ2
18-HEPE
6-trans,12-epi-LTB4
DPA
PGF2a
EPA
RvE4
AA
5-HETE
MaR1
8-iso-PGF2a
-log10(p)
log2(FC)
H
IgG RBC
CD47 Ab RBC
Component 2 (14%)
Component 1 (57%)
I
LXA4
4-HDHA
6-trans,12-epi-LTB4
LTB4
15R-LXA4
5-HETE
7-HDHA
18-HEPE
15d-PGJ2
RvE2
PGF2a
PGJ2
8-iso-PGF2a
5-HEPE
15-HETE
PGE2
-Log10(p)
Log2(FC)
G
LXA4
RvD4
17(R)-RvD3
4-HDHA
PGJ2
RvE2
15-deoxy-PGJ2
PGD2
6-trans,12-epi LTB4
PGF2α
DPA
18-HEPE
RvE4
MaR1
5(S)-HETE
8-iso-PGF2α
log2(FC) vs. Ctrl RBC
VIP score
J
4-HDHA
6-trans,12-epi LTB4
15(R)-LXA4
LXA4
LTB4
5-HETE
7-HDHA
15-deoxy-PGJ2
18-HEPE
8-iso-PGF2α
PGF2α
RvE2
PGJ2
5-HEPE
15(S)-HETE
PGE2
log2(FC) vs. IgG RBC
VIP score
K
AA
15(S)-HETE
LXA4
12/15-LOX
5-LOX
AA (pg/mg)
0.051
15-HETE (pg/mg)
0.058
LXA4 (pg/mg)
Ctrl RBC
Ox RBC
IgG RBC
CD47 Ab RBC

Figure 6

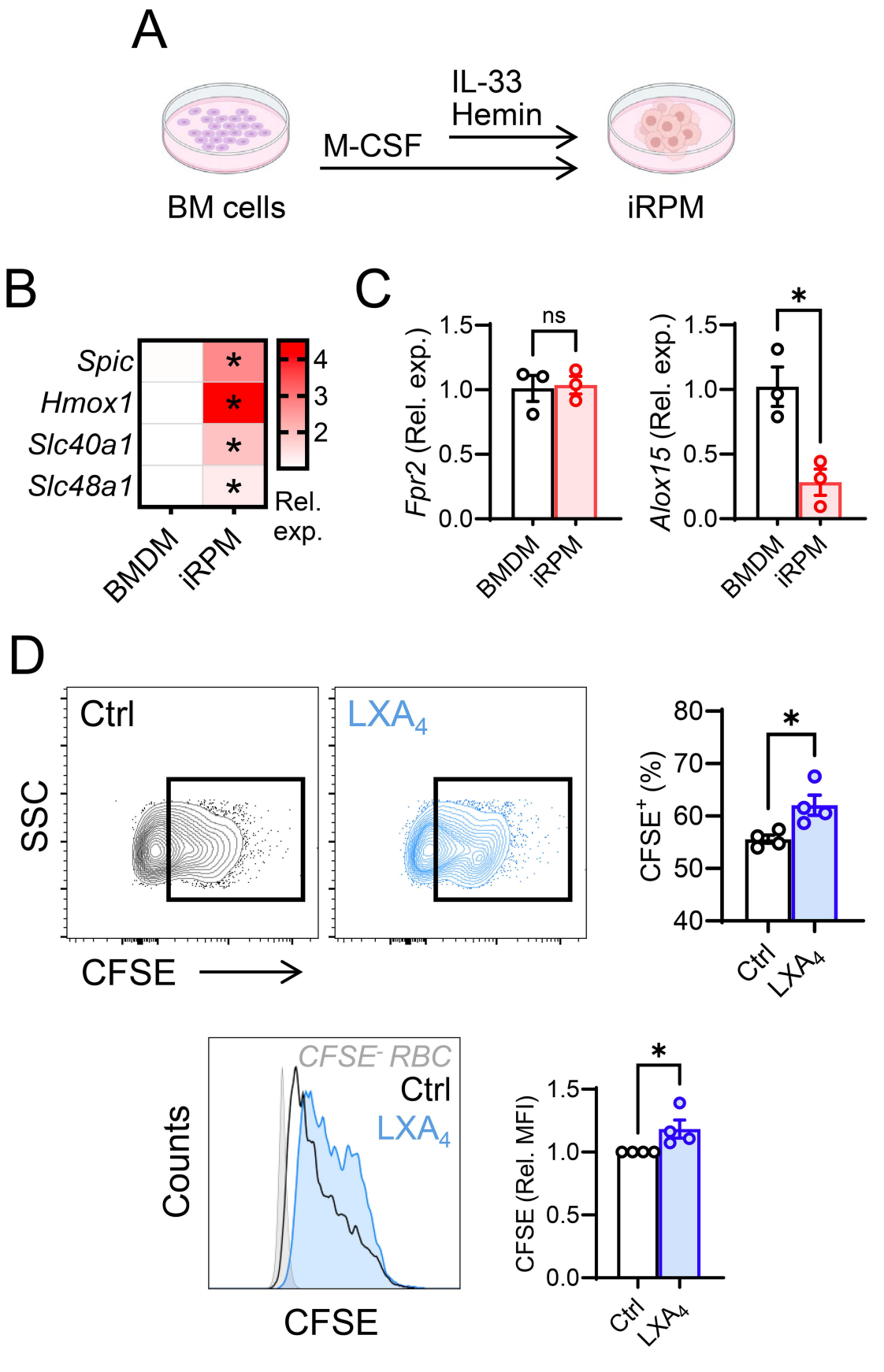
A
IL-33
Hemin
M-CSF
BM cells
iRPM
B
Spic
Hmox1
Slc40a1
Slc48a1
Rel. exp.
BMDM
iRPM
C
Fpr2 (Rel. exp.)
ns
Alox15 (Rel. exp.)
BMDM
iRPM
D
Ctrl
LXA4
SSC
CFSE
CFSE+ (%)
Ctrl
LXA4
CFSE- RBC
Ctrl
LXA4
Counts
CFSE
CFSE (Rel. MFI)
Ctrl
LXA4

Figure 7

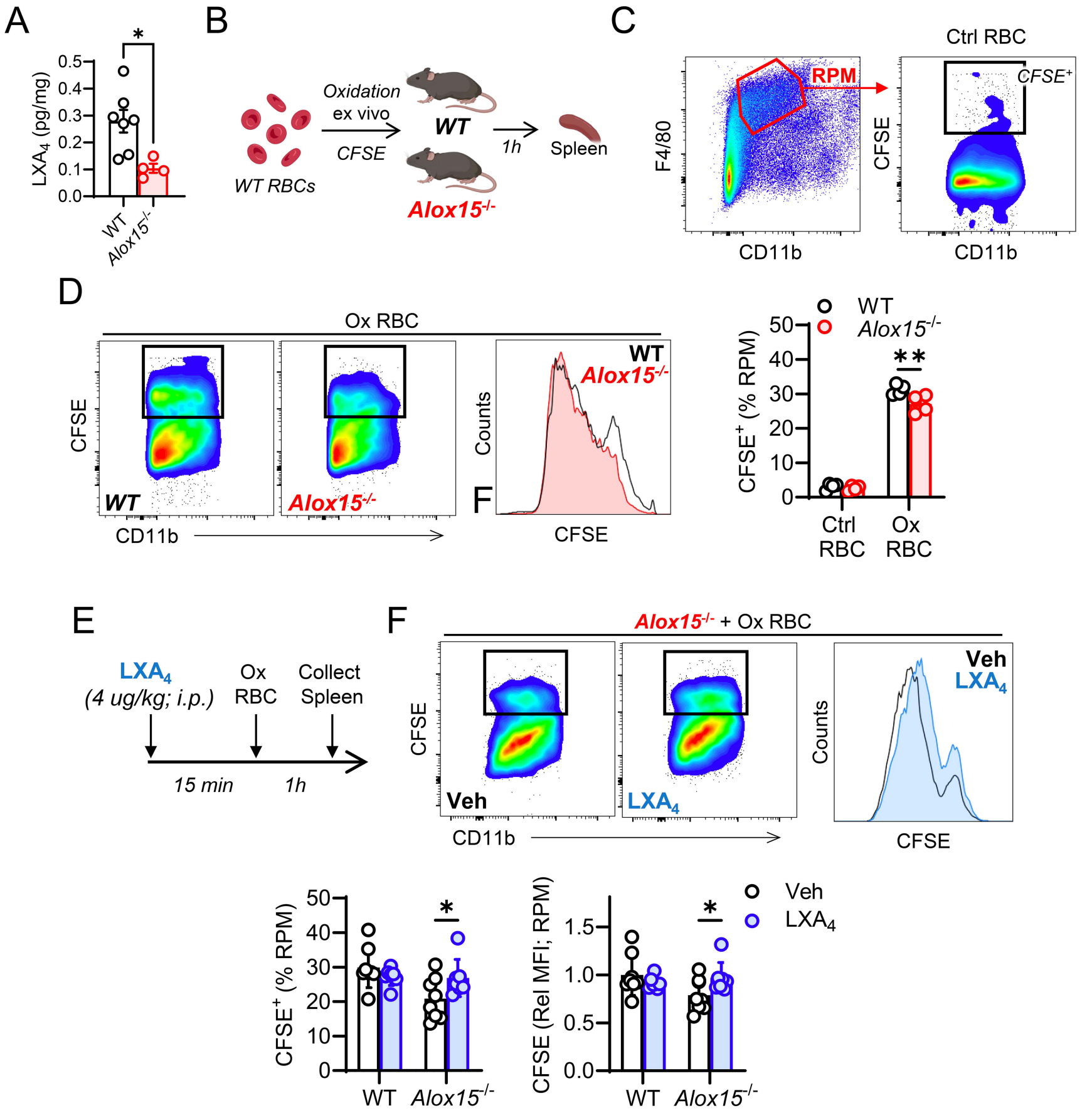
A
B
C
D
E
F
LXA4 (pg/mg)
WT
Alox15-/-
WT RBCs
Oxidation
ex vivo
CFSE
WT
Alox15-/-
1h
Spleen
Ctrl RBC
RPM
CFSE+
F4/80
CFSE
CD11b
Ox RBC
Counts
CFSE+ (% RPM)
Ctrl RBC
Ox RBC
LXA4
(4 ug/kg; i.p.)
Collect
Spleen
15 min
1h
Alox15-/- + Ox RBC
Veh
LXA4
CFSE (Rel MFI; RPM)

Title: Splenic erythrophagocytosis is regulated by ALX/FPR2 signaling

Authors: Haley Asplund[1], Hector H. Dreyer[1], Jing-Juan Zheng[1], Richa Singhal[1], Jason L. Hellmann[1], Brian E. Sansbury[1]

Affiliations:

1. Center for Cardiometabolic Science, Christina Lee Brown Envirome Institute, Division of Environmental Medicine, Department of Medicine, University of Louisville, Louisville, Kentucky, USA.

Short Title: LXA_4 regulates erythrophagocytosis

Keywords: proresolving lipid mediators, red pulp macrophages, red blood cell turnover

Correspondence to:

Brian E. Sansbury
Brian.Sansbury@Louisville.edu
580 S. Preston St., Room 304D Louisville,
KY 40202

SUPPLEMENTARY MATERIALS

1. Materials and Methods

1.1 Animals and Reagents

C57BL/6J (#00664), *Spic*-EGFP (#025673), LysM-Cre (#004781) and *Alox15*$^{-/-}$ (#002778) mice were purchased from The Jackson Laboratories (Bar Harbor, ME) at 10 to 16 weeks of age and allowed to acclimate for at least 1 week prior to inclusion in experimental studies or used as breeders. *Fpr2*$^{-/-}$ and humanized *ALX/FPR2-GFP* floxed (h*FPR2*$^{fl/fl}$) mice were provided by Idorsia Pharmaceuticals and bred in-house. All mice were maintained on normal laboratory chow diet, housed in a temperature controlled, 12-hour light–dark cycling environment, and were randomized to experimental groups. All animal procedures were performed in accordance with ethical regulations and pre-approved by the University of Louisville Institutional Animal Care and Use Committee. LXA_4 was purchased from Cayman Chemical (Ann Arbor, MI). Antibodies used for flow cytometry were purchased from BioLegend (San Diego, CA) and included: Streptavidin-FITC, F4/80-APC (BM8), CD11b-Brilliant Violet 421 (M1/70), CD47-PE (miap301), Ter119-Brilliant Violet 421 (TER-119), Ter119-PE (TER-119), CD71-APC (RI7217), CD45-FITC (S18009F), CD11b-FITC (M1/70), Gr1-FITC (RB6-8C5), DRAQ5, CD44-Brilliant Violet 711 (IM7).

1.2 *In vivo* RBC turnover

For *in vivo* tracking of circulating RBC, EZ-Link Sulfo-NHS Biotin (Thermo Scientific) was administered in a two-step labelling protocol, essentially as described[1,2]. Briefly, biotin was dissolved in water and further diluted in sterile saline prior to i.v. retro-orbital injection

(100 µl). In the first step, daily 1 mg biotin doses were administered for three days. Five days after the third administration, a second labelling dose of 0.6 mg was injected. Serial blood samples were collected via tail bleed at the indicated days and biotin expression was determined by flow cytometry.

1.2 Bone marrow erythroid precursors

Bone marrow from femur and tibia of WT and *Fpr2*$^{-/-}$ mice was flushed in cell staining buffer (BioLegend) using a 25G needle. Single cell solutions were obtained using a 70 µm cell strainer and subjected to flow cytometry analysis. Erythroid precursors were identified as CD45^{-}CD11b^{-}Gr1^{-}Ter119^{+}DRAQ5^{+}. Subpopulations of erythroblasts and reticulocytes were differentiated based on CD44 expression and cell size.

1.3 Histology

Spleens were collected and fixed in 10% neutral buffered formalin prior to being embedded in paraffin wax. Tissue sections (5 µM) were deparaffinized and stained with Mayer's Hematoxylin (Electron Microscopy Sciences, PA, USA) and Eosin Y Solution (Sigma-Aldrich, MO, USA), or with Prussian blue (Abcam, UK) according to manufacturer's instructions. For immunofluorescence staining, deparaffinized sections were rehydrated prior to antigen retrieval using a citrate buffer and incubation with Anti-F4/80-APC rat monoclonal antibody (clone: BM8; BioLegend). Imaging and analysis were performed using a Keyence BZ-X810 fluorescence microscope (IL, USA).

1.4 Gene Expression Analysis

1.4.1 RNA-Sequencing

An antibody-based magnetic bead isolation kit (Stem Cell Technologies) was used according to manufacturer's instructions to obtain F4/80$^+$ cells from whole spleen. Total RNA was isolated from mouse spleen and F4/80$^+$ splenocytes using the RNeasy Plus Universal Mini Kit (Qiagen). RNA quality was evaluated using NanoDrop ONEC (Thermo Scientific) and then subjected to poly-A RNA sequencing. RNA integrity was assessed using the Bioanalyzer 2100 system (Agilent Technologies, CA, USA). For library construction, the abclonal second strand synthesis module kit was utilized (Cat. # RK20346). Equimolar pooling of libraries was performed based on Q.C. values, and paired-end sequencing was performed on an Illumina NovaSeq X Plus (Illumina, California, USA) using the 25B Flow Cell. FASTQ files were generated utilizing BCL2fastq.

1.4.2 Bioinformatics analysis

Quality control (Q.C.) of the raw sequence data was performed using FastQC (version 0.10.0) for each sequencing sample. The sequences were aligned to the mm10 mouse reference genome using STAR version 2.6 [3]. Differential expression of ENSEMBL protein-coding transcripts was performed using DESeq2[4], and raw counts were obtained from the STAR-aligned bam format files using HTSeq version 0.10.0[5]. The raw counts were normalized using the Relative Log Expression (RLE) method and then filtered to exclude genes with fewer than ten counts across the samples. DESeq2 guidelines were used to identify differentially expressed genes, and all P values were adjusted for testing multiple genes (Benjamini–Hochberg procedure; $p \leq 0.05$). Functional

enrichment analysis was performed using the clusterProfiler R package to identify enriched Gene Ontology biological processes for each set of differentially expressed genes (DEGs)[6]. RNA-seq data have been deposited in the NCBI GEO database with the accession numbers GSE292685 and GSE292686.

1.4.3 qRT-PCR

RNA from flow cytometry-sorted or differentiated macrophages was isolated using RNeasy Plus Universal Mini Kit (Qiagen) according to manufacturer's instructions. cDNA was synthesized using Applied Biosystems High-Capacity cDNA Reverse Transcription Kit and qPCR was performed with Applied Biosystems PowerUp SYBR Green Master Mix (Thermo Fisher Scientific) on an Applied Biosystems QuantStudio 5. RT^2 qPCR Primer Assays (Qiagen) were used for each target gene and relative expression was determined using the $2^{-\Delta\Delta Ct}$ method normalized to expression of *Hprt*.

1.5 *In vivo* splenic RBC uptake

Erythrophagocytosis *in vivo* was assessed essentially as described[7,8]. Blood was collected from a naïve donor mouse via cardiac puncture and mixed with 0.2 M EDTA. RBC were separated from plasma by centrifugation at 3,500 rpm for 10 minutes at 4°C and washed twice with PBS. Washed RBC were resuspended in PBS and either oxidized with copper(ii) sulfate ($CuSO_4$) and L-ascorbic acid or incubated with CD47 blocking antibody. For oxidation, RBC were incubated in 0.2 mM $CuSO_4$ and 5 mM L-ascorbic acid in PBS at 4% hematocrit for 30 minutes at 37°C, with gentle agitation every 10 minutes. After incubation, RBC were washed twice with PBS containing 5 mM EDTA followed by two washes with PBS alone. For CD47 antibody blockage, RBC were

incubated with 10 µg/mL CD47 antibody (Bio X Cell) or 10 µg/mL mouse IgG isotype control (Bio X Cell, BE0083) for 1 hour at 37°C. Treated RBC were labeled with carboxyfluorescein succinimidyl ester (CFSE; BioLegend, CA, USA) according to the manufacturer's instructions. Briefly, $1x10^8$ cells/mL were incubated with 5 µM/mL CFSE in PBS for 20 minutes at room temperature then washed with PBS. CFSE-labeled RBC ($2x10^8$ cells) were administered to mice via retro-orbital injection (200 µL sterile saline). After 1 hour, mice were euthanized and spleens collected for flow cytometry. A single cell suspension was generated using a 70 µM cell strainer with PBS using the plunger from a 5 mL syringe. The suspension was centrifuged and resuspended in Cell Staining Buffer (BioLegend). Cells were incubated in 2 µg Fc-block (BioLegend) for 5-10 minutes, stained with fluorescent antibodies for 15-20 minutes, and fixed in 1% paraformaldehyde. Data were acquired using a BD Fortessa X-20 Flow Cytometer and analyzed using FlowJo software.

1.6 Targeted lipidomics

1.6.1 Tissue preparation and solid phase extraction (SPE)

All reagents used in lipid mediator extractions and analyses were LC/MS grade, ensuring the highest level of purity. Spleens were removed from animals and placed directly in ice-cold methanol containing commercially available deuterium-labeled synthetic standards (PGE_2-d4, 15d-PGJ_2-d4, LTB_4-d4, LXA_4-d5, 11,12-EET-d11, 15-HETE-d8, 5-HETE-d8, RvE1-d4, RvD2-d5, RvD3-d5, MaR1-d5, and MaR2-d5; Cayman Chemical, Ann Arbor, MI, USA), then stored at -80°C. Prior to lipid extraction, tissue was minced with surgical

scissors on ice and then centrifuged (13,000 rpm; 10 min; 4°C). The supernatant was collected and subjected to solid phase extraction (SPE) essentially as described previously[9]. Briefly, samples were acidified to a pH of 3.5 and added to C18 SPE columns (Biotage, Uppsala, Sweden) that were conditioned with successive washes of methanol and water. Neutral lipids were removed from the column using *n*-hexanes while lipid mediators were eluted with methyl formate. Using N_2 gas, the solvent was evaporated and samples resuspended in methanol:water (50:50, v/v).

1.6.2 LC-MS/MS analysis

Extracted lipid mediator samples were analyzed using a Shimadzu (Kyoto, Japan) liquid chromatography system (LC 20-AD with an SIL-20AC autoinjector) coupled to a QTrap5500 mass spectrometer (AB Sciex, Framingham, MA, USA) operated in negative polarity mode. Samples were injected onto a Kinetex Polar C18 HPLC column (100 mm x 3 mm x 2.6 µm; Phenomenex, CA, USA) held at 59°C. A gradient elution of methanol:water:acetic acid beginning at 45:55:0.01 (v/v/v) and ending at 80:20:0.01 (v/v/v) was used at a flow rate of 0.5 ml/min. Data was acquired using Analyst software (v 1.7.1) and analyzed with Sciex OS-Q. Identified mediators had matching chromatographic peak retention time with that of synthetic standards run in parallel (+/- 0.1 min), signal:noise ratio >5, and an on-column calculated concentration above the lower limit of quantification for each mediator. Fragmentation spectra of synthetic standards compared with that of samples was also used. Absolute quantification was achieved by comparing samples to a 12-point standard curve of synthetic standards run

in parallel. SCIEX OS (v.2.0.1) software was used for peak identification and quantification.

1.6.3 Data analysis

Statistical analyses were performed using the freely available Metaboanalyst software platform (Metaboanalyst.ca). Analytes with missing data in more than 50% of samples in both experimental groups were excluded from analysis. Missing values were imputed with 1/5 the minimum value of that analyte. Data were then log transformed and autoscaled prior to downstream analyses (partial least squares discriminant, volcano plot, VIP).

1.7 iRPM differentiation

Differentiation of iRPM was performed essentially as described[10]. Briefly, murine bone marrow was isolated and plated in RPMI-1640 (Thermo Fisher) supplemented with 10% heat-inactivated FBS, 1% penicillin-streptomycin, and 20 ng/mL M-CSF (StemCell Technologies). On day 4, media was supplemented with IL-33 (10 ng/mL; BioLegend) and hemin (20 μM; Sigma-Aldrich). After 5 additional days, cells were ready for experiments. For gene expression studies, BMDM were generated using M-CSF media without hemin and IL-33.

2. References

1. Khandelwal, S. & Saxena, R.K. Assessment of survival of aging erythrocyte in circulation and attendant changes in size and CD147 expression by a novel two step biotinylation method. Exp Gerontol. 2006;41(9):855-861.
2. Saxena, R.K., Bhardwaj, N., Sachar, S.*, et al.* A Double in vivo Biotinylation Technique for Objective Assessment of Aging and Clearance of Mouse Erythrocytes in Blood Circulation. Transfus Med Hemother. 2012;39(5):335-341.
3. Dobin, A., Davis, C.A., Schlesinger, F.*, et al.* STAR: ultrafast universal RNA-seq aligner. Bioinformatics. 2013;29(1):15-21.
4. Love, M.I., Huber, W. & Anders, S. Moderated estimation of fold change and dispersion for RNA-seq data with DESeq2. Genome Biol. 2014;15(12):550.
5. Anders, S., Pyl, P.T. & Huber, W. HTSeq--a Python framework to work with high-throughput sequencing data. Bioinformatics. 2015;31(2):166-169.
6. Yu, G., Wang, L.G., Han, Y.*, et al.* clusterProfiler: an R package for comparing biological themes among gene clusters. OMICS. 2012;16(5):284-287.
7. Sambrano, G.R., Parthasarathy, S. & Steinberg, D. Recognition of oxidatively damaged erythrocytes by a macrophage receptor with specificity for oxidized low density lipoprotein. Proc Natl Acad Sci U S A. 1994;91(8):3265-3269.
8. Turpin, C., Meilhac, O., Bourdon, E.*, et al.* Methodologies and tools to shed light on erythrophagocytosis. Biochimie. 2022;202(166-179.
9. Dalli, J., Colas, R.A., Walker, M.E.*, et al.* Lipid Mediator Metabolomics Via LC-MS/MS Profiling and Analysis. Methods Mol Biol. 2018;1730(59-72.
10. Lu, Y., Basatemur, G., Scott, I.C.*, et al.* Interleukin-33 Signaling Controls the Development of Iron-Recycling Macrophages. Immunity. 2020;52(5):782-793 e785.

3. Figure Legends

Supplementary Figure 1. Bone marrow erythropoiesis. Representative flow cytometry dot plots and quantification of erythroid precursors in the bone marrow of WT and *Fpr2*$^{-/-}$ mice. n = 6-7 per group. Data are mean ± SEM. *p<0.05 as determined by unpaired Student's t-test.

Supplementary Figure 2. Erythrocyte parameters of complete blood count analysis in WT and *Fpr2*$^{-/-}$ mice. Quantification is shown. Data are mean ± SEM. n = 34 per group. *RBC – red blood cell count, Hb – hemoglobin, HCT – hematocrit, MCV – mean corpuscular volume, MCH – mean corpuscular hemoglobin, MCHC – mean corpuscular hemoglobin concentration, RDW – red cell distribution width*

Supplementary Figure 3. Flow cytometry gating of splenic red pulp macrophages. Representative flow cytometry dot plots of spleens of WT and *Spic*-EGFP mice. GFP+ cells cluster into a population of CD11b^{dim}F4/80^{+} cells.

Supplementary Figure 4. Validation of myeloid-specific hALX/FPR2 knockout mice. (**A**) Humanized *FPR2-GFP* knockin floxed mice (h*FPR2*$^{fl/fl}$) were crossed with mice expressing Cre recombinase under the Lysozyme M promoter (LysM-Cre) to generate mice with myeloid-specific deletion of *FPR2* (h*FPR2*^{MKO}). (**B**) Representative PCR gel electrophoresis used for genotyping of h*FPR2*^{MKO} colony. (**C**) Expression of GFP and human ALX/FPR2 was determined in peripheral blood leukocytes by flow cytometry using Ly6C and Ly6G to identify monocytes and neutrophils, respectively.

Supplementary Figure 5. Quantification of CFSE+ cells in spleens after adoptive transfer of oxidized (Ox) or CD47 blocking antibody (CD47 Ab) treated RBC. Data

are mean ± SEM. n = 4-6 per group. ns: $p>0.05$ as determined by unpaired Student's t-test.

Supplementary Figure 6. Chromatograms from Arachidonic Acid Metabolome. Representative extracted ion mass chromatograms are shown for arachidonic acid-derived lipid mediators that were significantly changed in spleens after adoptive transfer of damaged red blood cells. A representative synthetic standard is shown in addition to a sample. Shaded area illustrates the peak area that was used for quantitation.

Supplementary Figure 7. Chromatograms from Docosahexaenoic Acid, Docosapentaenoic Acid, and Eicosapentaenoic Acid Metabolomes. Representative extracted ion mass chromatograms are shown for docosahexaenoic, docosapentaenoic, and eicosapentaenoic acid-derived lipid mediators that were significantly changed in spleens after adoptive transfer of damaged red blood cells. A representative synthetic standard is shown in addition to a sample. Shaded area illustrates the peak area that was used for quantitation.

Supplementary Figure 1

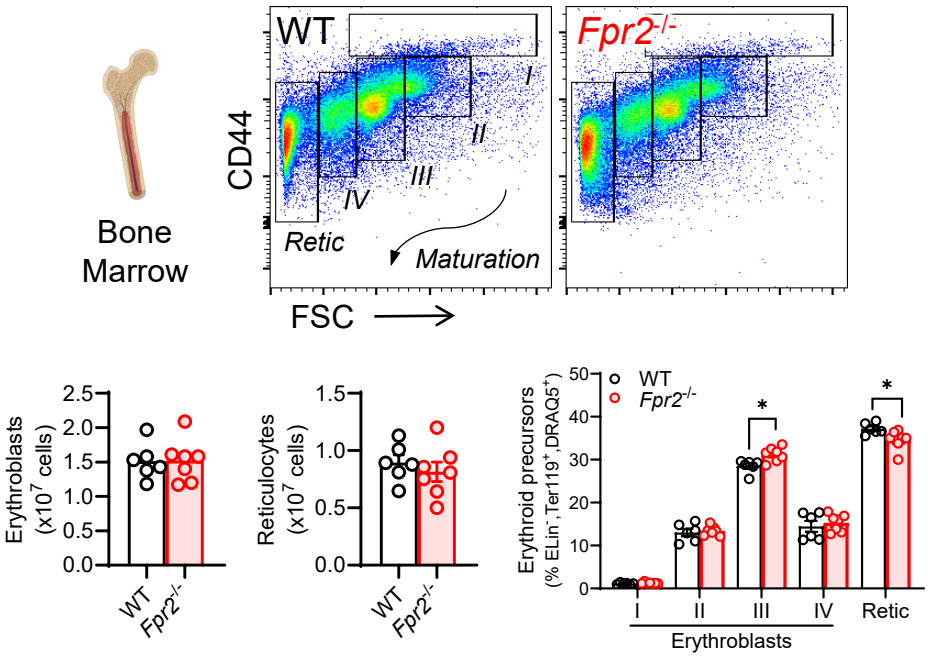

Supplementary Figure 2

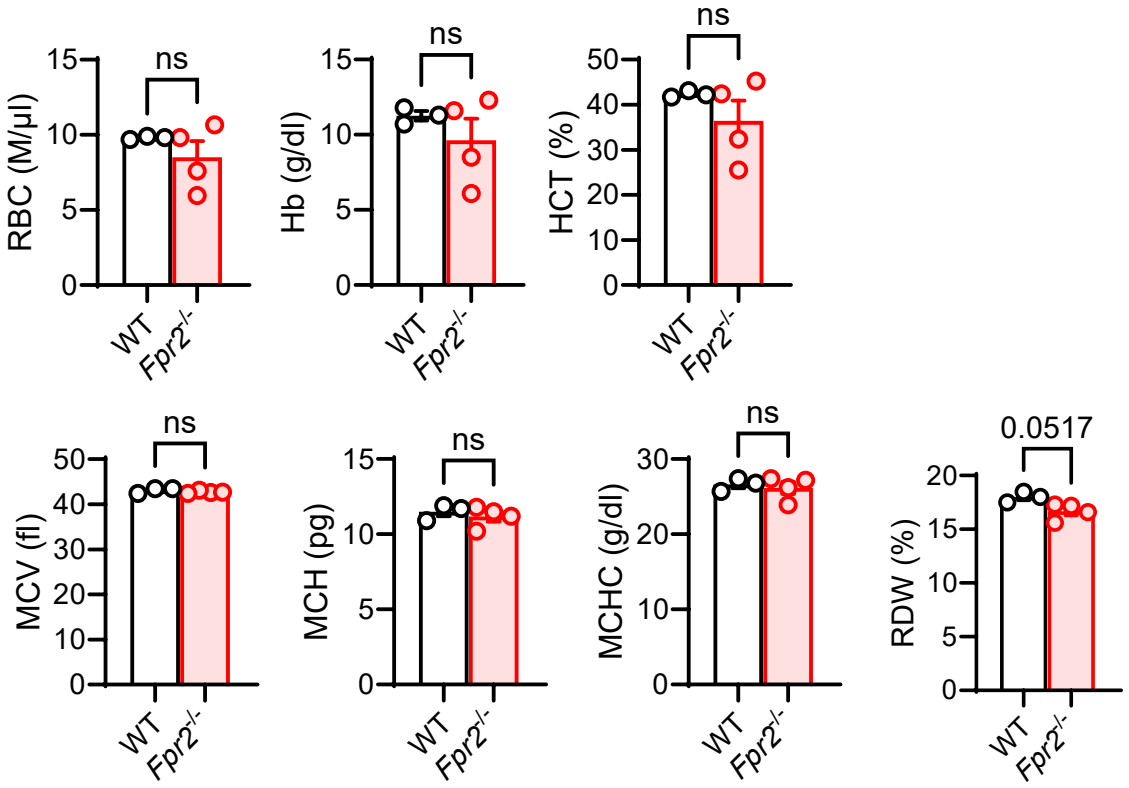

Supplementary Figure 3

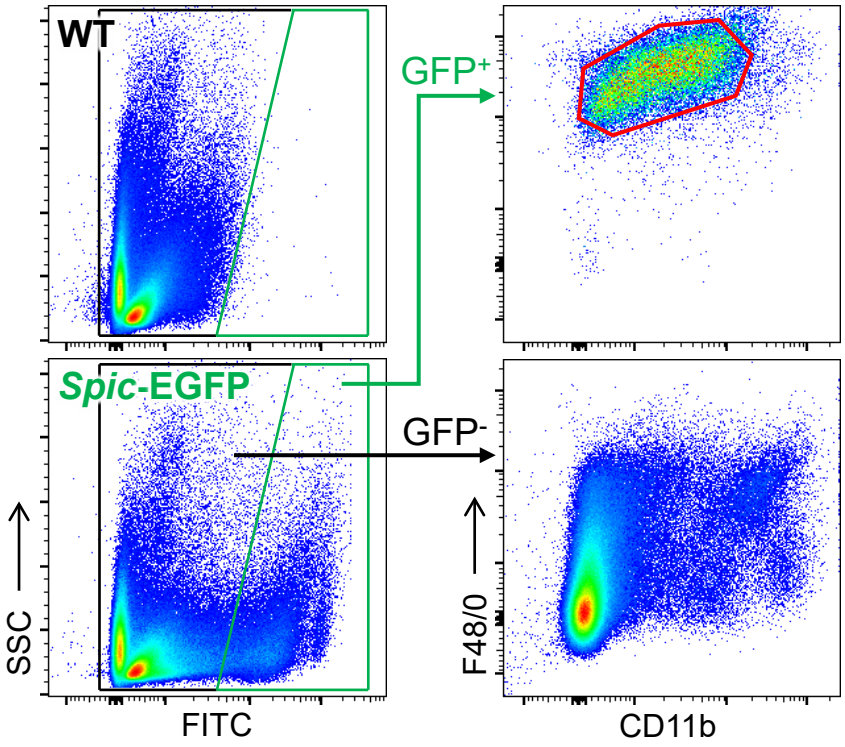

Supplementary Figure 4

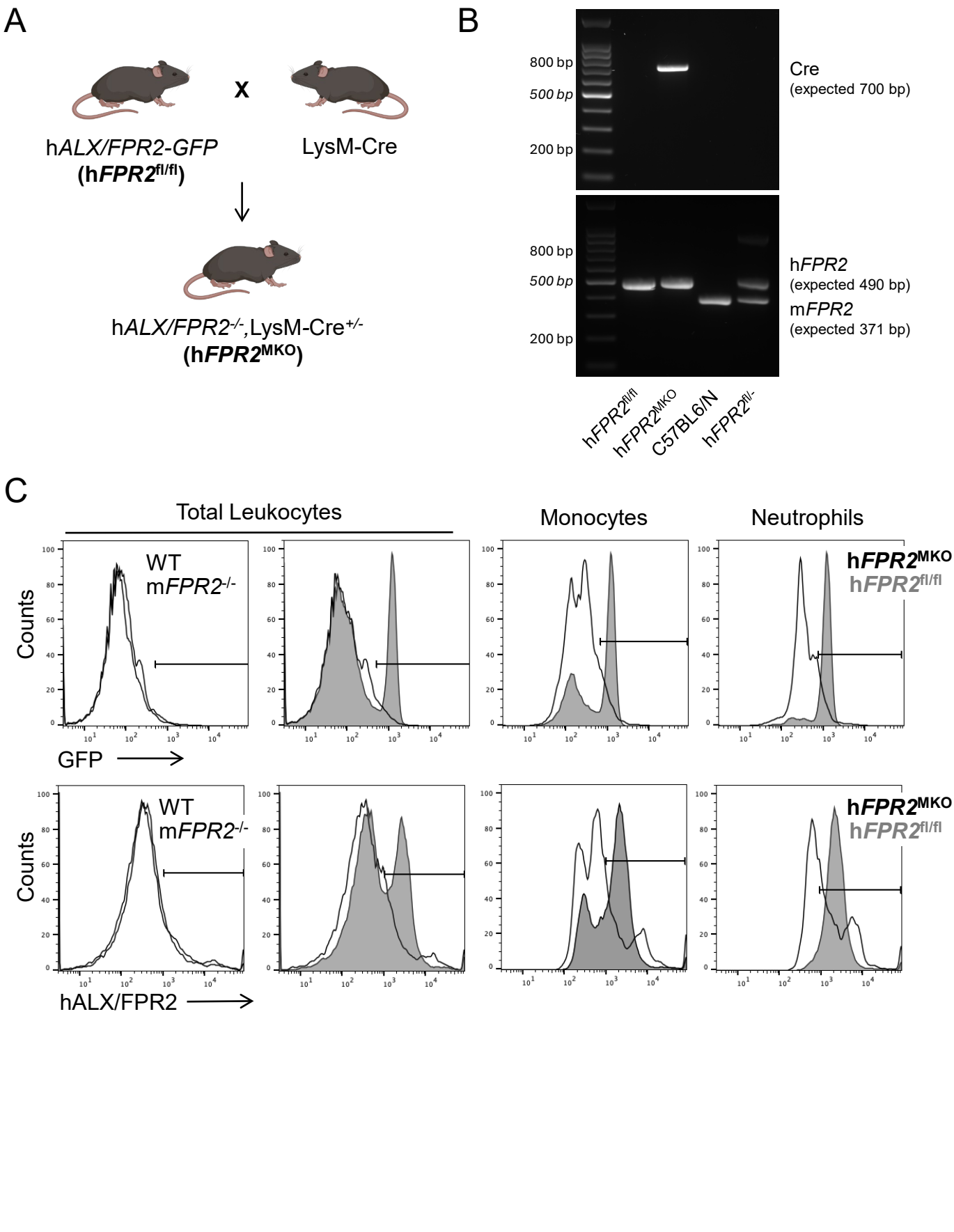

Supplementary Figure 5

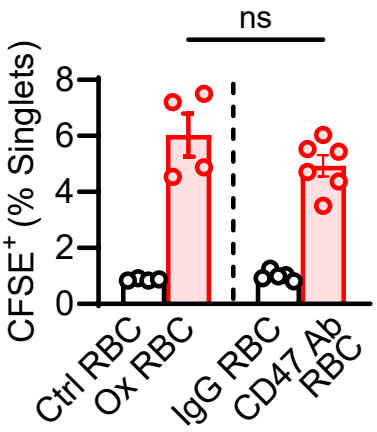

Supplementary Figure 6

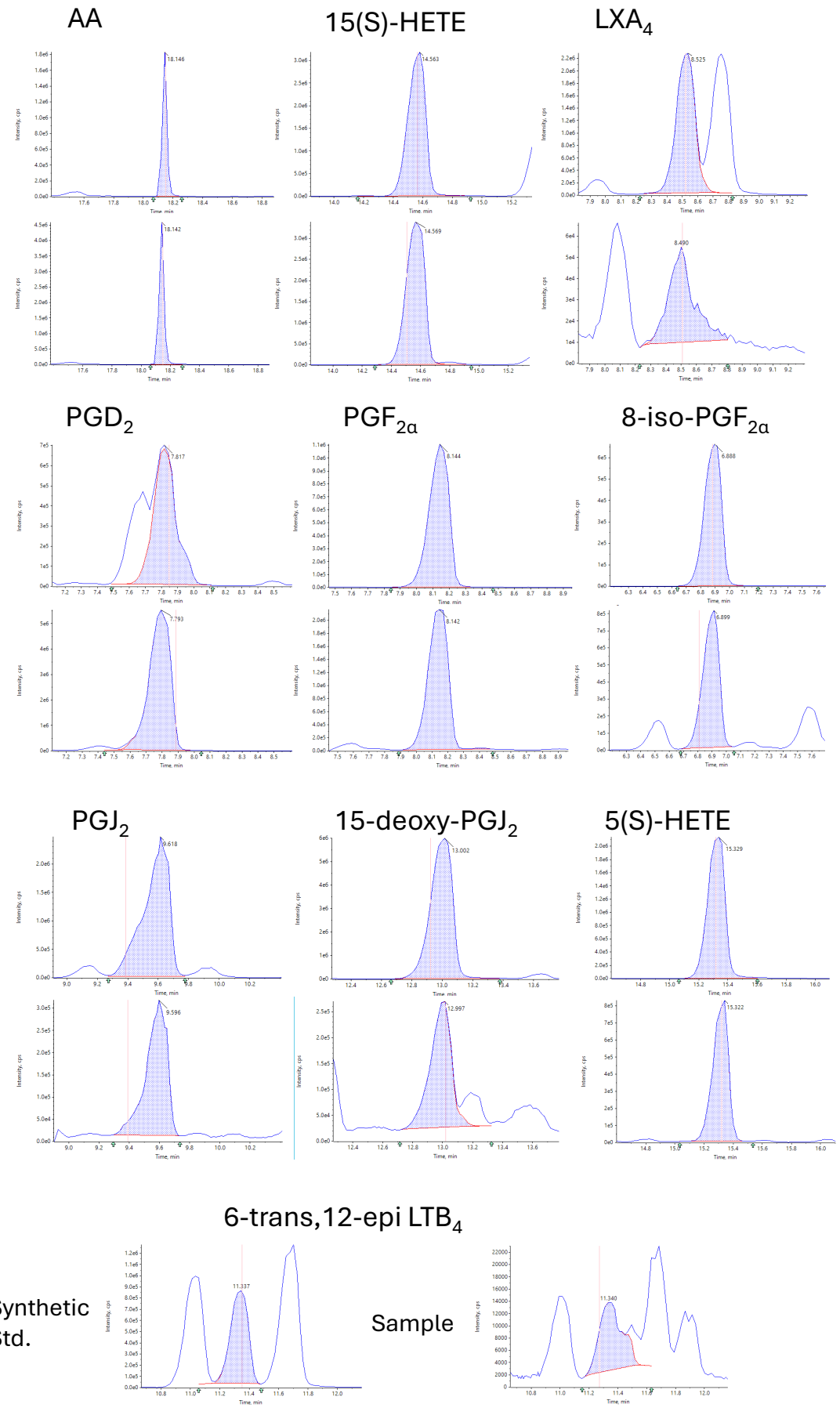

Supplementary Figure 7